THE JOURNAL OF PHYSICAL CHEMISTRY A

Article

pubs.acs.org/JPCA

Collisional Energy Transfer in Highly Excited Molecules

Paul L. Houston,*[,†,‡] Riccardo Conte,[§] and Joel M. Bowman[§]

[†]School of Chemistry and Biochemistry, Georgia Institute of Technology, 901 Atlantic Drive, Atlanta, Georgia 30332, United States

[‡]Baker Laboratory, Department of Chemistry and Chemical Biology, Cornell University, Ithaca, New York 14852, United States

[§]Department of Chemistry and Cherry L. Emerson Center for Scientific Computation, Emory University, Atlanta, Georgia 30322, United States

Supporting Information

ABSTRACT: The excitation/de-excitation step in the Lindemann mechanism is investigated in detail using model development and classical trajectory studies based on a realistic potential energy surface. The model, based on a soft-sphere/line-of-centers approach and using elements of Landau−Teller theory and phase space theory, correctly predicts most aspects of the joint probability distribution $P(\Delta E,\Delta J)$ for the collisional excitation and de-excitation process in the argon−allyl system. The classical trajectories both confirm the validity of the model and provide insight into the energy transfer. The potential employed was based on a previously available ab initio intramolecular potential for the allyl fit to 97418 allyl electronic energies and an intermolecular potential fit to 286 Ar−allyl energies. Intramolecular energies were calculated at the CCSD(T)/AVTZ level of theory, while intermolecular energies were calculated at the MP2/AVTZ level of theory. Trajectories were calculated for each of four starting allyl isomers and for an initial rotational level of $J_i = 0$ as well as for J_i taken from a microcanonical distribution. Despite a dissimilarity in Ar−allyl potentials for fixed Ar−allyl geometries, energy transfer properties starting from four different isomers were found to be remarkably alike. A contributing factor appears to be that the orientation-averaged potentials are almost identical. The model we have developed suggests that most hydrocarbons should have similar energy transfer properties, scaled by differences in the potential offset of the atom−hydrogen interaction. Available data corroborate this suggestion.

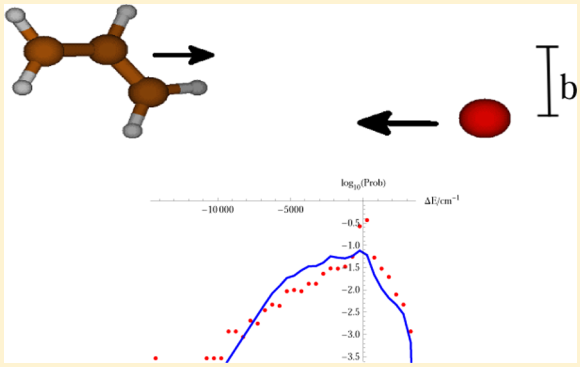

I. INTRODUCTION

The Lindemann mechanism, now nearly a century old,[1,2] is essential to understanding many processes of fundamental importance because it describes the chemical transformation in which a molecule isomerizes or dissociates to products. It has two seemingly simple steps:

$$A + B \rightleftharpoons A + B^*, \quad (k_1/k_{-1}) \tag{R1}$$

$$B^* \rightarrow \text{products}, \quad (k_{uni}) \tag{R2}$$

where A is typically an atom or small molecule, B is the target molecule, and B* is the target molecule with vibrational and/or rotational excitation. The study of unimolecular dissociation has followed two important routes since the initial surge of interest in this process during the 1920s.[1,2] In the first route of investigation, studies of isolated molecules using excitation techniques that provide a known energy, often exciting the molecule to a selected electronic/vibrational/rotational state, have provided a wealth of information concerning how the product distribution in (R2) depends on the total energy. Experimental and theoretical advances in the 1980s have made it possible also to detect the final state distribution, the angular distribution of products with respect to the polarization of the dissociating light, and the angular momentum alignment of the products.[3−5] On the other hand, most dissociations occur under conditions where the excited molecule typically suffers one or more collisions before dissociation, gaining or losing internal energy and angular momentum during the process. Thus, the second route for investigation of molecular collisions has been to characterize the collisional energy transfer in (R1). Since the rate of dissociation through any open channel increases with internal vibrational energy, collisional effects can either increase or decrease the dissociation yields, depending on whether the collision results in vibrational excitation or relaxation, respectively. The competition between these processes is usually described by a master equation analysis.[6]

This paper studies the process (R1) in detail, using model development and classical trajectory studies to gain insight into both how and why a molecule is excited or de-excited in a collision. Many results of the argon−allyl classical trajectory studies starting with $J_i = 0$ have been discussed in a previous paper.[7] The previous paper in this journal presents further allyl−argon results for $J_i \neq 0$ and also investigates how

Received: June 22, 2014
Revised: August 4, 2014
Published: August 12, 2014

properties of the excitation/de-excitation affect the product distribution in (R2).[8]

Experimental techniques have shed much light on the process of collisional energy transfer in highly excited molecules.[9−31] Among these techniques are chemical activation reaction systems,[9] time-resolved spontaneous infrared fluorescence,[10−12] time-resolved ultraviolet absorbance,[13−15] kinetically controlled selective ionization (KCSI),[27] high-resolution transient IR absorption spectroscopy,[28,29] mass spectroscopy,[30] and time-sliced ion imaging.[31] Trajectory calculations based on realistic potential energy surfaces have also enhanced our understanding of both the unimolecular dissociation of isolated molecules and the collisional energy transfer that occurs in competition with dissociation.[32−41]

Theoretical models and simple expressions that describe the energy transfer process are an essential ingredient of a master equation analysis. Thus, much effort has been devoted to developing functions for that use. The functions usually describe the target molecule at the microcanonical level (E,J) but describe the collision by a temperature. The field has been reviewed several times, notably by Troe[42,43] in 1977, by Gilbert in 1991,[44] by Barker and colleagues in 2001,[45] by Barker and Golden in 2003,[6] and Barker and Weston, Jr. in 2012.[35]

Gilbert[44] considers several phenomenological models for the probability of energy transfer $P(E,E')$, where E' is the initial total energy and E is the final total internal energy. These include (i) an exponential down model, (ii) a biased random walk model, (iii) a strong collision model, and (iv) an impulsive ergodic collision theory. Several of these have features that agree with experimental data, where available, in predicting the "average down energy", the energy lost averaged over all the collisions for which the total energy decreases. Troe[42,43] has proposed a double exponential model or a double biexponential form, one for the collisions that increase energy and one for the collisions that decrease energy. The two are related by detailed balance. Barker and Golden and Barker and colleagues, respectively, mention several semiempirical methods for categorizing data.[6,45] Barker and Weston, Jr.[35] note that several groups have attempted to simplify the two-dimensional joint probability distribution, $P(\Delta J,\Delta E)$ to a one-dimensional version, including Marcus[46] and Smith and Gilbert.[47,48] However, a central point of their article is that such simplification is not yet possible using the methods proposed so far. They propose an empirical formula for the joint probability distribution that includes the sum of two exponential functions and has ten parameters. The biexponential form has been proposed by others as well.[19,36,37,49,50] A principle aim of this previous work has been to develop expressions that can be used in master equation analysis.

Developing physical models for the energy transfer is a somewhat different aim. Earlier work includes the approach by Nordholm and colleagues,[51−58] who apply ergodic collision theory to the energy transfer problem, and by Barker,[59] who applies SSH theory. Both have had some success in predicting $P(E,E')$ probabilities and moments. Of particular note is the application of partially ergodic collision theory (PECT) to azulene and biphenylene.[60] The ergodic collision theory (ECT)[51] assumes that the collision is "strong", that is, that the activation and deactivation leaves the reactant molecule in a completely relaxed state. The probability of being found in any particular state is described by the canonical ensemble at the temperature of the medium. The partially ergodic collision theory[56,57] used for azulene and biphenylene accounts for the fact that collisions are not always so strong as assumed in the ECT model. It introduces a collisional efficiency parameter β_E and assumes complete equilibrium for only a subset of the degrees of freedom, called the "active degrees." With these adjustments, the fit to the data is excellent.[60]

The work to be reported below also develops a physical model for the energy transfer. Whereas the previous models have been either statistically based or based solely on SSH theory, our theory is a simple soft-sphere/line-of-centers model consisting of a Landau−Teller type treatment of the vibrational energy transfer and a phase-space treatment of the rotational energy transfer. It appears to fit the major features of the joint probability distribution obtained from trajectory calculations we have performed on the allyl radical.[8] These calculations were performed at the microcanonical level for both the target molecule and the collision. An initial simplification is to treat the target molecule as a sphere, since in that approximation the vibrational and rotational energy transfer are separable in a line-of-centers treatment. We will see, however, that this is not as severe a limitation as might be thought. Methods for extending the model are considered in Conclusions.

The remainder of the article is organized as follows. In Model for Collisional Energy Transfer in Highly Excited Molecules, we develop the model for collisional energy transfer, and in Potential Surfaces and Trajectory Methods, we outline the methodology of the trajectory calculations. Results provides a summary of comparisons between the model predictions and the trajectory calculations, with substantial reference to the Supporting Information. Discussion goes over the assumptions of the model and compares its predictions to the results of several previous trajectory studies. The Summary provides Conclusions and areas for further research.

II. MODEL FOR COLLISIONAL ENERGY TRANSFER IN HIGHLY EXCITED MOLECULES

A. Development of the Model. We start by enumerating assumptions of the model: (a) The essential features can be described by an orientation-averaged interaction potential $V(R)$. (b) The rotational energy for a state J can be characterized by $B_{sph}J(J+1)$, where B_{sph} is a spherically averaged rotational constant calculated from the spherical moment of inertia, $I = (2/3)\sum m_i r_i^2$, where r_i is the distance of the mass m_i from the center of mass. This assumption is equivalent to spreading the mass of each atom evenly over the surface of a sphere at the atom's distance from the center-of-mass and then calculating the moment of inertia. We will use B_{sph} to mean the actual spherically averaged rotational constant, while the term B_{rot} will denote the rotational constant that is used in a given context. The ratio will be $B_{ratio} = B_{rot}/B_{sph}$. (c) Vibrational energy can be transferred to/from the target molecule during the collision in any amount consistent with conservation of energy [i.e., the vibrational frequency distribution of the molecule (its density of vibrational states) is smooth as a function of frequency]. We assume that the density of vibrational states increases with energy as $\rho(E) = E^{(s-1)+(1/2)}$, as used elsewhere[35] and discussed by Holbrook, Pilling, and Robertson.[61] Here, s is $3N$-6 ($3N$-5), where N is the number of atoms in the target molecule. (d) Energy transfer does not occur if the energy evaluated along the line of centers is negative. (e) Rotational energy transfer is governed by a simple phase-space model and is caused by a change in the orbital angular momentum of the collision system as evaluated

dx.doi.org/10.1021/jp506202g | J. Phys. Chem. A 2014, 118, 7758−7775

using the velocity along a line perpendicular to the line of centers.

At the microcanonical level, we develop a semiclassical theory for vibrational energy transfer based on the adiabaticity principle. The essential equation for the exchange of vibrational energy is $P_{f\leftarrow i} \sim \exp(-\tau_c/\tau_v)$, where $P_{f\leftarrow i}$ is the probability for going from state i to state f, τ_v is the vibrational period, and τ_c is the collision time. The model is based on first-order perturbation theory as outlined in standard textbooks (e.g., section 8.6.2 of ref 62). It is part of the development of the Landau–Teller theory[63,64] and is derived from the basic physical idea that for energy transfer to have high probability, there must be a Fourier component of the force at the frequency of vibration.

In the original Landau–Teller approach, the change of energy was given by $\Delta E_{vib} = h\nu$; there was only one vibrational frequency. Using assumption (c), we generalize to let ΔE_{vib} be a continuous variable; that is, the target molecule is assumed to be so excited that its frequency spectrum is continuous with an amplitude at any frequency or energy given by the density of states, $\rho(E_i)$. Since $1/\tau_v$ is the vibrational frequency, the change vibrational energy in wavenumbers is $1/\tau_\nu = c\Delta E_{vib}$, where c is the speed of light. Thus,

$$P_{f\leftarrow i} \sim \frac{\rho(E_i + \Delta E_{vib})}{\rho(E_i)} \exp[-|\Delta E_{vib}|c\tau_c] \quad (1)$$

where the absolute value is introduced (as in eqs 4.2, 4.10, and 4.13 of ref 64) because the probability is expected to decrease whether ΔE_{vib} is positive or negative. Multiplication by the ratio of the density of states between the "receiving" vibrational level, $E_i + \Delta E_{vib}$, and the initial excitation level, E_i, is included since the rate is expected to depend linearly on the density of receiving vibrational levels. It remains to determine the collision time, τ_c.

The collision time can be taken as a distance of atomic dimensions, d_{force}, divided by the component of the relative velocity along the line of centers. The line-of-centers approach is similar to that used for standard derivations of simple collision theory [e.g., section 3.3.1 of ref 62], except that instead of a hard sphere, we have a collision with a softer potential $V(R)$. We then decompose the incoming velocity, v_{rel}, into two orthogonal components: v_{loc} along the line of centers between the incoming atom and the center of mass of the target at the turning point, and $v_{perploc}$ along a direction perpendicular to the line of centers. These motions correspond to energies $E_{loc} = (1/2)\mu v_{loc}^2$ and $E_{perploc} = (1/2)\mu v_{perploc}^2$, where $E_{loc} + E_{perploc} = E_{rel}$, and μ is the reduced mass of the collision pair. The potential $V(R)$ typically has both a repulsive region extending to R_0, where $V(R_0) = 0$ and an attractive region extending from R_0 to infinity. For collision of an atom with the target molecule characterized by a velocity corresponding to $E_{rel} = (1/2)\mu v_{rel}^2$, the location of the turning point, TP, is given by the solution to the equation

$$V[R(\mathrm{TP})] = E_{rel}\left(1 - \frac{b_{rep}^2}{\mathrm{TP}^2}\right) = E_{loc} \quad (2)$$

Here, b_{rep} is the impact parameter with respect to a potential offset, r_{offset}, defining the outer shell of the target molecule [$V(r_{offset}) = E_{rel}$] rather than centered on the center-of-mass of the target molecule, as shown in Figure 1. This formulation is consistent with the assumptions of the Landau–Teller model, where, for a collision A + B − C, the (exponential) potential is between B and A.[62]

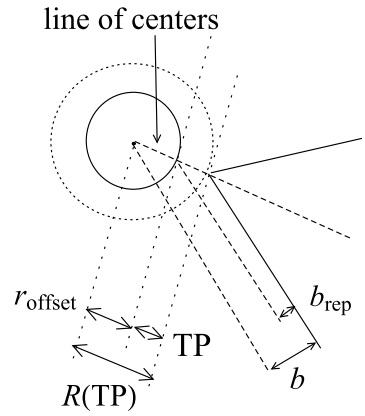

Figure 1. The solid circle is the spherically averaged potential surface for the target molecule. The impact parameter with respect to the center of the target molecule is b, whereas the impact parameter with respect to the center of the repulsive potential at the surface of the sphere is b_{rep}. The radius of the target molecule is r_{offset}, given as the distance at which the potential energy is equal to E_{rel}, the relative translational energy. The turning point in the trajectory, TP, is the value of b_{rep} at which the potential energy is equal to the energy evaluated along the line of centers. R(TP) is the distance of the turning point from the center of the target molecule, and TP is the distance between r_{offset} to the turning point. The turning point is the location where $V[R(\mathrm{TP})] = E_{loc}$.

The TP value when $b_{rep} = 0$ is 0, and it then increases with b_{rep}, eventually reaching the point TP = b_{rep} when $b_{rep} = R_0 - r_{offset}$. Beyond this distance, $b_{rep} >$ TP, the energy along the line of centers is negative, and the relative velocity along the line of centers is thus imaginary. With negative energy along the line of centers, we assume that energy transfer cannot occur (assumption d). An important consequence of this assumption is that the potential in the attractive region does not matter for energy transfer; we need to know the potential $V(R)$ only between r_{offset} and R_0. In this region, $\tau_c = \tau_c(b_{rep},E_{rel}) = d_{force}/\{(2E_{rel}/\mu)[1 - (b_{rep}^2/\mathrm{TP}^2)]\}^{1/2} = d_{force}/v_{loc}(b_{rep}, E_{rel})$. This completes the calculation of how the probability for vibrational energy transfer depends on impact parameter, relative translational energy, initial excitation E_i, and ΔE_{vib}. When the potential $V(R)$ is an exponential decreasing with R/s_{range}, the distance d_{force} is equal to s_{range}.[62] For other potentials, it seems likely that d_{force} should be given by $d_{force} = -V(r_{offset})/[\mathrm{d}V(R)/\mathrm{d}R]_{R\rightarrow r_{offset}}$. The result for vibrational energy transfer is

$$P_{vib}(b_{rep}, E_{rel}) = \frac{\rho(E_i + \Delta E_{vib})}{\rho(E_i)} \times \exp\left[-|\Delta E_{vib}|c\frac{d_{force}}{v_{loc}(b_{rep}, E_{rel})}\right] \quad (3)$$

where the dependence on E_{rel} and b_{rep} is explicitly noted.

Rotational transfer has been considered in detail by many others (e.g., refs 65–70). While most of these models are more complex than is warranted by the current theory, several conclusions are worth noting. Rotational transfer can be thought of as the product of a probability for the energy transfer ΔE_{rot} and a probability for the angular momentum transfer $|\Delta J| = |J_f - J_i|$. McCaffery and colleagues argue that the

dx.doi.org/10.1021/jp506202g | J. Phys. Chem. A 2014, 118, 7758–7775

former probability should be close to unity.[69] The latter probability is shown to fall exponentially as $|\Delta J|$ increases. Thus, any prediction of the model should be in accord with these ideas.

We develop a rotational energy transfer model from the line-of-centers approach used above. If the energy along the line of centers is given by the rhs of (2), the remaining energy is due to velocity perpendicular to the line of centers,

$$v_{\mathrm{perploc}} = \sqrt{(2E_{\mathrm{rel}}/\mu)(b_{\mathrm{rep}}^2/\mathrm{TP}^2)} \quad (4)$$

The energy associated with this velocity is $E_{\mathrm{perploc}} = (1/2)\mu v_{\mathrm{perploc}}^2$. When the target molecule is spherical, as assumed here, the velocity along the line of centers can excite vibrational motion but not rotation, whereas the velocity perpendicular to the line of centers can excite rotational motion but not vibration. Note from Figure 1 that v_{perploc} has an impact parameter $R(\mathrm{TP}) = r_{\mathrm{offset}} + \mathrm{TP}(b_{\mathrm{rep}})$ with respect to the center of mass of the molecule and an impact parameter TP relative to the offset position, where $V(r_{\mathrm{offset}}) = E_{\mathrm{rel}}$.

The potential experienced by motion perpendicular to the line of centers is shown in Figure 2, where the red line indicates

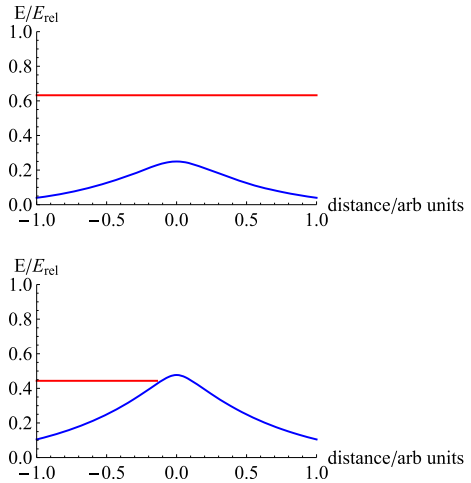

Figure 2. $E_{\mathrm{perploc}}/E_{\mathrm{rel}}$ (red line) and barrier as a function of arbitrary distance. Only the amount of E_{perploc} that falls below the peak of the barrier $V[R(\mathrm{TP})] = E_{\mathrm{loc}}$ can be used for rotational excitation. When $E_{\mathrm{perploc}} > V[R(\mathrm{TP})] = E_{\mathrm{loc}}$, the energy $E_{\mathrm{perploc}} - V[R(\mathrm{TP})]$ remains in translation.

the energy perpendicular to the line of centers. The peak of the potential occurs at the turning point, and the value at the peak is given by $V[R(\mathrm{TP})]$, which from eq 2 is equal to E_{loc}. When $E_{\mathrm{perploc}} < E_{\mathrm{loc}}$, as in the bottom panel, then all of it can be used for rotational excitation. When $E_{\mathrm{perploc}} > E_{\mathrm{loc}}$, then the difference in energy, $E_{\mathrm{perploc}} - E_{\mathrm{loc}}$ remains in translational energy, while E_{loc} is available for rotational excitation. Whichever amount of rotational energy is available, the maximum change in angular momentum is due to the reversal of the velocity associated with that rotational energy, since for energies less than or equal to that of the peak potential, the velocity decreases during the collision and then reverses itself. Consequently, the maximum angular momentum available for rotational excitation is $\Delta J_{\mathrm{max}} = 2\mu v_L[r_{\mathrm{offset}} + \mathrm{TP}(b_{\mathrm{rep}})]$, where $(1/2)\mu v_L^2$ = the smaller of $\{E_{\mathrm{perploc}}, E_{\mathrm{loc}}\}$. For conservation of angular momentum $|J_f - J_i| \leqslant \Delta J_{\mathrm{max}}$.

We now use a phase space model to evaluate the probability for a transition from J_i to J_f.[71,72] A given ΔJ_{max} can give rise to a number of final rotational states. It seems reasonable that the probability of giving rise to a particular J_f should be proportional to the number of ways to form that J_f divided by the number of ways to form any final rotational level. The states are best enumerated as their projections onto the axis of the initial orbital angular momentum. The initial state, J_i, has projections m_{Ji} from $-J_i$ to J_i. The magnitude of the orbital angular momentum change is equal to the change in the magnitude of the rotational angular momentum ΔJ. This transforms the projections m_{Ji} to the range of either $(-J_i + \Delta J)$ to $(J_i + \Delta J)$ or $(-J_i - \Delta J)$ to $(J_i - \Delta J)$. The final rotational state must have projections that fall in these ranges. In the former case, J_f must be at least as big as $J_i + \Delta J$, while in the latter it must be at least as big as $J_i - \Delta J$. On the other hand, J_f cannot be larger than these values because, if it were, conservation of angular momentum would be violated for alignments where J_i and J_f have their maximum projection onto the axis of initial angular momentum. Thus, $J_f = J_i \pm \Delta J$. Note that when $\Delta J > J_i$, it is possible for the final rotation to be in a direction opposite to the original rotation. In this case, the formula for $J_f = J_i \pm \Delta J$ would give a negative value, even though J_f is allowed. Thus, for the magnitudes, $J_f = |J_i \pm \Delta J|$. Because we will be most interested in the limits of J_f given particular values of ΔJ_{max} and J_i, we will be most interested in the situation where both J_i and J_f have their maximum possible projections onto the angular momentum axis. In this case, the projection is equal to the magnitude.

The range of possible ΔJ can be understood using Figure 3, which plots ΔJ as a function of b_{rep}. The values of ΔJ_{max} as a

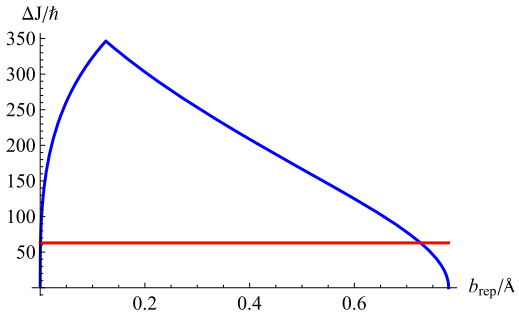

Figure 3. ΔJ in units of $\hbar$ as a function of b_{rep}. The blue curve gives ΔJ_{max} as a function of b_{rep} for $E_{\mathrm{rel}} = 3500\ \mathrm{cm}^{-1}$ (10.0 kcal mol). $J_i = 200$, $J_f = 137$ and for the GM isomer. The red horizontal line is at the lowest value of $\Delta J = |J_f - J_i| = J_i - J_f$, where angular momentum is conserved. In this particular example, $|J_f - J_i| = J_i - J_f = 63$.

function of b_{rep} are shown by the blue curve, in this example for $E_{\mathrm{rel}} = 3500\ \mathrm{cm}^{-1}$ (10.0 kcal/mol) and for the GM isomer. The red horizontal line is at the lowest value of $\Delta J = |J_f - J_i|$, for which angular momentum can be conserved; that is, given J_i and ΔJ_{max} where the red line intersects the blue curve, a value of the final rotational level lower than J_f cannot conserve angular momentum. The blue line at $\Delta J = \Delta J_{\mathrm{max}}$ is the maximum ΔJ available from the collision; it depends on b_{rep}.

When ΔJ is equal to $J_i - J_f$ at the red line, conservation of angular momentum is just possible. At higher ΔJ, J_f is just one of many final states that could be formed. In this view, all of ΔJ_{max} could be used for rotational excitation, but it would produce other final states in addition to J_f. Let the possible final states be called J_x. For each value of ΔJ between the red line at $J_i - J_f$ and the blue line at ΔJ_{max}, there are two possible final J values given by the formula discussed above: $J_x = |J \pm \Delta J|$.

dx.doi.org/10.1021/jp506202g | J. Phys. Chem. A 2014, 118, 7758−7775

What this means physically is that, when $J_x = J_i + \Delta J$, the initial rotation of the sphere is in the same direction as the initial orbital angular momentum; the collision increases the rotation. When $J_x = J_i - \Delta J$, the initial rotation of the sphere is in the opposite direction from the initial orbital angular momentum; the collision decreases rotation. Note that if $\Delta J > J_i$, the decrease will produce a final state that is rotating in the opposite direction from the initial rotation; in this case, the collision has not only decreased J_i but has also reversed its direction. The absolute value in $J_x = |J \pm \Delta J|$ corrects the magnitude to always be ≥ 0.

We now determine the range of final states J_x consistent with angular momentum conservation. If $\Delta J_{max} < J_i$ then the lowest possible J_{xmin} is $J_i - \Delta J_{max}$ and the maximum possible final state is $J_{xmax} = J_i + \Delta J_{max}$. If $\Delta J_{max} \geq J_i$ then the lowest possible J_{xmin} is 0 but the final states can range up to $J_{xmax} = J_i + \Delta J_{max}$ for situations where J_i is decreased but not reversed and from 0 to $\Delta J_{max} - J_i$ for situations where J_i is reversed. Both ranges must be included since they arise from distinct values of ΔJ.

Having now determined which J_x final states would be available for a particular ΔJ_{max}, we simply need to add them up weighted by their overall degeneracy. Because we have assumed a spherical rotor, the overall degeneracy of a state with J_x is $(2J_x + 1)^2$. Thus, the probability for the J_f state is the ratio between the $(2J_f + 1)^2$ degeneracy of J_f and the sum over J_x of the $(2J_x + 1)^2$ degeneracies for each J_x:

$$P_{rot}(J_i, J_f, \Delta J) = \frac{(2J_f + 1)^2}{\delta_1 \sum_{Jx=J_i-\Delta J_{max}}^{J_i+\Delta J_{max}} (2J_x + 1)^2 + \delta_2 \sum_{Jx=0}^{J_i+\Delta J_{max}} (2J_x + 1)^2 + \delta_2 \sum_{Jx=0}^{\Delta J_{max}-J_i} (2J_x + 1)^2} \quad (5)$$

where $\delta_1 = 1$ if $J_i \geq \Delta J_{max}$ and 0 otherwise, and $\delta_2 = 1$ if $J_i < \Delta J_{max}$ and 0 otherwise. It should be noted that ΔJ_{max} depends not only on b_{rep} but on E_{rel}, μ and on the potential through the turning points. The summations can easily be evaluated using

$$\sum_{Jx=J_{xmin}}^{J_{xmax}} (2J_x + 1)^2 = \frac{1}{3}(1 + J_{xmax} - J_{xmin}) \times (3 + 8J_{xmax} + 4J_{xmax}^2 + 4J_{xmin} + 4J_{xmax}J_{xmin} + 4J_{xmin}^2) \quad (6)$$

Further illustration of the rotational theory is provided in Appendix SI of the Supporting Information, where it is shown that this simple model gives rise to a probability for rotational excitation and de-excitation that is very similar to one that falls off nearly exponentially with $|\Delta J|$, at least in ranges of $|\Delta J|$ that are not further limited by conservation laws. Figure SI-5 of the Appendix of the Supporting Information shows an example.

The overall probability will be P_{vib} times P_{rot} times a function Δ_{EAM} whose value is unity if the collision conserves energy and angular momentum and zero otherwise. Conservation of angular momentum is implicit in the development of P_{rot}: $|J_f - J_i| \leqslant \Delta J_{max}$. Conservation of energy is somewhat more complicated. We assume that all of E_{loc} can, in principle, be converted to vibrational energy, with the probabilities determined by (3) and (5). However, not all of $E_{perploc}$ can be converted to rotational energy. From Figure 2 we note that when $E_{perploc} > E_{loc}$, the difference in energy $E_{final} = E_{perploc} - E_{loc}$ must be included in the final translational motion. Conservation of energy requires that when $E_{perploc} > E_{loc}$, $\Delta E \leqslant E_{rel} - E_{final}$ or $\Delta E \leqslant E_{rel} - E_{perploc} + E_{loc}$, where $\Delta E = \Delta E_{vib} + \Delta E_{rot}$ is the total change in internal energy. Figure SI-2a of the Supporting Information illustrates this point. Since $E_{perploc}$ and E_{loc} depend on impact parameter, the conservation of energy equation must be evaluated at each impact parameter.

The final equation for the joint probability distribution of having $\Delta E = \Delta E_{vib} + \Delta E_{rot}$ and $\Delta J = J_f - J_i$ is then given by

$$JPD[J_i, J_f, \Delta E, b_{rep}, E_{rel}, d_{force}, B_{rot}, \mu] = \Delta_{EAM}(b_{rep}) P_{vib}(b_{rep}) P_{rot}(b_{rep}) \quad (7)$$

This equation must be integrated over b_{rep} to obtain the total cross section,

$$\sigma(E_{rel}) = \int_0^{b_{rep,max}} JPD[J_i, J_f, \Delta E, b_{rep}, E_{rel}, d_{force}, B_{rot}, \mu] 2\pi b_{rep}\, db_{rep} \quad (8)$$

To obtain the joint probability distribution as a function of temperature, $\sigma(E_{rel})$ should be divided by the hard sphere cross section $\pi b_{rep,max}^2$ and integrated over E_{rel} using the energy distribution function $G(E_{rel})$, given, for example, in eq 1.37 of ref 62. Alternatively, the rate constant $k(T)$ may be obtained by multiplying $\sigma(E_{rel})$ by v_{rel} and integrating the result over E_{rel}.

Several comments are worth noting. Given a potential, $V(R)$, and the reduced mass, μ, the joint probability distribution has no other adjustable parameters. The offset, r_{offset}, is determined from the potential as the distance at which $V(r_{offset}) = E_{rel}$ and B_{sph} is simply determined from the spherical moment of inertia, $I = (2/3)\sum m_i r_i^2$, where r_i is the distance of the mass m_i from the center of mass. Furthermore, the intermolecular potential $V(R)$ appears only through determination of r_{offset} and through the variation in turning point with b_{rep}. Finally, the only region of the potential that is important is in the distance range from r_{offset} to R_0. Further comments on the model and its assumptions will be deferred until Discussion of the Assumptions.

B. Simplifications and Scaling Properties of the Model. While the evaluation of the above model is exact, it is obvious that the model is an oversimplification of the real physics of molecular energy transfer. We discuss the assumptions in more detail in Discussion of the Assumptions, but it is worth noting here that the model can both be simplified and cast in a somewhat more general way that maintains the proper scaling of probability with input parameters (B_{sph}, E_{int}, μ) but allows for adjustments to account for more realistic collisions.

We start with the following generalizations. We assume that even when the potential is of the form $\exp[-R/s_{range}]$, the value of d_{force} in (3) may not be exactly equal to s_{range}. Rather, we let $d_{force} = a_{vib} s_{range}$, where a_{vib} is a dimensionless coefficient whose value would be unity if the model were exact. A second generalization is to assume that $\Delta J_{max} = 2\mu v_L[r_{offset} + TP(b_{rep})]$ is also scaled by a dimensionless parameter, where we redefine ΔJ_{max} as $\Delta J_{max} = 2\mu v_L[r_{offset} + TP(b_{rep})]/a_{rot}$. Again, a_{rot} would be equal to unity if the original model were exact. Finally, there are good reasons why the actual rotational constant should be somewhat smaller than B_{sph}, as discussed in Discussion of the Assumptions. Thus, we define B_{ratio} as $B_{rot} = B_{ratio} B_{sph}$, where

dx.doi.org/10.1021/jp506202g | J. Phys. Chem. A 2014, 118, 7758−7775

B_{rot} is the actual rotational constant, B_{sph} is the spherically averaged rotational constant, and B_{ratio} is a dimensionless parameter that would be equal to unity if the model were exact. These three adjustable parameters, a_{vib}, a_{rot}, and B_{ratio}, can be used to account for inaccuracies in the model when applied to real systems. The formulas, however, maintain the proper scaling with relation to E_{int}, μ, etc.

We now simplify the model by estimating the results of the integration over impact parameter, b_{rep}. In practice, this simplification greatly speeds the calculation, which often includes further averaging over relative collision energy and the initial rotational state. The following are the steps in simplification.

We simplify the collision by assuming that the energies along and perpendicular to the line of centers are constant values instead of values that depend on impact parameter. We set both equal to $E_{av} = E_{rel}/2$. The velocities along these directions are thus also equal and given by $v_{av} = (2E_{av}/\mu)^{1/2}$. We further assume that the potential can be written in the form $V(R) = (E_{rel} + \epsilon)\exp[-(R - r_{offset})/s_{range}] - \epsilon$, at least in the region between the R where $V(R) = E_{rel}$ and the R where $V(R) = 0$.

The vibrational energy transfer is then simply

$$P_{vib2} = [\rho(E_i + \Delta E_{vib})/\rho(E_i)] \times \exp[-a_{vib}(1.4)|\Delta E_{vib}|s_{range}/v_{av}] \quad (9)$$

where $a_{vib} = d_{force}/s_{range}$ is a dimensionless adjustable parameter that would be unity for close agreement with the original model, and the factor of 1.4 is an empirically derived correction for the fact that the average of $(1/v)$ is larger than the reciprocal of the average of v.

The rotational energy transfer would normally depend on the area under $P_{rot}(b_{rep})$ from $b_{rep,min}$ to $b_{rep,max}$, where $P_{rot} = (2J_f + 1)^2$/sum, and sum is the denominator of eq 5; it depends on $\Delta J_{max}(b_{rep})$. Instead, we take $\Delta J_{max}(b_{rep})$ to be constant with b_{rep} and equal to $\Delta J_{maxav} = \mu v_{av}\text{offset}_{av}/a_{rot}$, where offset_{av} replaces $[r_{offset} + TP(b_{rep})]$ and is obtained from $\text{offset}_{av} = r_{offset} + R'$, where R' is the solution to $V(R') = E_{av}$. With these approximations, the rotational energy transfer probability is given simply by

$$P_{rot2} = (2J_f + 1)^2/(1/3(1 + 2\Delta J_{maxav}) \times (3 + 12J_i + 12J_i^2 + 4\Delta J_{maxav} + 4\Delta J_{maxav}{}^2) \quad (10)$$

The integration over b_{rep} is evaluated by using conservation of angular momentum to determine the limits of the integration. These limits are from b_1 to b_2, where b_1 and b_2 are the two impact parameters where $|\Delta J|$ intersects the blue curve (see Figure 3). We replace the blue curve by a triangle whose apex is at $(1/6)(R_0 - r_{offset})$. Defining $R_{rot} = |\Delta J|/\Delta J_{maxav}$, it can be shown that $b_1 = R_{rot}(1/6)(R_0 - r_{offset})$ and $b_2 = (R_0 - r_{offset})[1 - (5/6)R_{rot}]$. For an integrand P_{rot2} that is constant with b_{rep}, the integral is simply $P_{rot2}(b_2^2 - b_1^2)/(R_0 - r_{offset})^2$ or $P_{rot2}[1 - (5/3)R_{rot} + (2/3)R_{rot}^2]$.

Conservation of energy is still governed by a delta function, but it takes a somewhat different form when no longer dependent on b_{rep}:

$$\Delta_2 = \begin{cases} 10^{-8} & |J_f - J_i| > \Delta J_{maxav} \\ 1 & |J_f - J_i| \le \Delta J_{maxav} \\ 10^{-8} & \Delta E > E_{rel} \\ 1 & \Delta E \le E_{rel} \\ 1 - \exp[-0.1(E_{rel} - \Delta E)/\Delta E] + 10^{-8} & \Delta E \ge 0 \text{ and } E_{rel} \ge \Delta E \\ 1 & \Delta E < 0, \text{ or } E_{rel} < \Delta E \end{cases} \quad (11)$$

where zero probability has been replaced by 10^{-8} so as to prevent problems in taking the log for plotting purposes. The first and second pairs of lines in (11) ensure conservation of angular momentum and energy, respectively. The last pair of lines is a replacement for the condition $\Delta E \leqslant E_{rel} - E_{final}$, discussed above. The falloff in probability with increasing ΔE_{vib} or increasing $|J_f - J_i|$ is steeper as a_{vib} or a_{rot} increase, respectively.

The final probability is obtained by multiplying the three functions of (9), (10), and (11) by the result for the integration over b_{rep}:

$$JPD_2 = \Delta_2 P_{vib2} P_{rot2}[1 - (5/3)R_{rot} + (2/3)R_{rot}^2] \quad (12)$$

The joint probability distribution given in (12) is unnormalized; normalization on a grid of $\{J_f, \Delta E\}$ can be performed to either set the maximum probability to unity or to set the sum of all probabilities to unity. Alternatively, the probability of (12) may be divided by $\{(2J_i + 1)^2/(1/3)(1 + 2\Delta J_{maxav})(3 + 12J_i^2 + 4\Delta J_{maxav} + 4\Delta J_{maxav}{}^2)\}$ so that the probability for $\{E_{vib} = 0, \Delta J = 0\}$ is unity. Figures S2−S8 of the Supporting Information show that the approximate value of (12) is in good agreement with the numerical solution (8) for argon collisions with GM allyl over a range of J_i from at least 0 to 280 and over E_{rel} from at least 100 cm^{-1} (0.29 kcal/mol) to 7000 cm^{-1} (20.0 kcal/mol).

An advantage of (12) over (8) is that it is much faster for calculations. On a single laptop processor using 46 bins in energy and 16 bins for the final rotational level, (8) takes about 20−30 min for the rather complex intermolecular potential we use for argon interacting with allyl. On the other hand, the use of (12) takes only 20 s for accuracy that is nearly comparable (see Figures S2−S8 of the Supporting Information). When additional integration over relative energy is needed to simulate a temperature, and/or if integration over initial J_i is needed, then the calculation time grows substantially so that the speed-up factor of roughly 60 is helpful.

Equations 8 and 12 do not obey detailed balance, but if desired, it is easy to impose it. For a microcanonical system, detailed balance implies the $g_i k_{if} = g_f k_{fi}$, where $g_i(g_f)$ is the degeneracy of the initial (final) state, k_{if} is the rate constant from the initial state to the final state, and k_{fi} is the rate constant for the reverse process. Given the same relative velocity and hard sphere cross section for the forward and reverse rates, detailed balance may also be written in terms of probabilities: $g_i P_{if} = g_f P_{fi}$. The vibrational part of the energy transfer does obey detailed balance. For the vibrations, the degeneracy factors are proportional to the density of states, and the forward and reverse rate constants are related by a change in the sign of ΔE_{vib} in (3). Inspection quickly shows that P_{if}/P_{fi}

dx.doi.org/10.1021/jp506202g | J. Phys. Chem. A 2014, 118, 7758−7775

$= \rho(E_i + \Delta E_{vib})/\rho(E_i - \Delta E_{vib}) = g_f/g_i$, as required. The rotational part of the energy transfer does not obey detailed balance, as can be seen from (10) and (12). For the forward process, $g_i P_{if} = (2J_i + 1)^2 P_{J_i \to J_f} = (2J_f + 1)^2/\text{denom}(J_i)$, whereas for the reverse process $g_f P_{fi} = (2J_{f+1})^2 P_{J_f \to J_i} = (2J_i + 1)^2/\text{denom}(J_f)$, where denom($J_k$) is defined as the denominator of (10) with J_i replaced by J_k. The ratio of $g_f P_{if}/(g_i P_{if})$ is thus not equal to unity, as required by detailed balance, but instead equal to denom(J_f)/denom(J_i). The reason for this is that phase space theory itself is not designed to satisfy detailed balance. Detailed balance can be imposed on the theory by replacing J_i in the denominator of (10) by the average of J_i and J_f. We note that the factor in (12) that accounts for the integration over impact parameter is invariant to exchange of J_i and J_f, and since the vibrational part of the problem obeys detailed balance, the final equations will obey detailed balance if it is imposed on the denominator of (10). For practical purposes, it is not really necessary to do so because the ratio $g_f P_{if}/(g_i P_{if})$ is never far from unity. Numerical tests on GM allyl show that even when the spread between J_i and J_f is ±150, the ratio changes only between 0.64 and 2.07. Because the energy transfer varies by many orders of magnitude over this range, plots such as those to be shown below are virtually unchanged by imposing detailed balance.

In summary, formulas (9)−(12) allow an efficient calculation of the joint probability distribution. When the dimensionless values a_{vib}, a_{rot}, and B_{ratio} are all equal to unity, the result is very close to the prediction of the original model.

III. POTENTIAL SURFACES AND TRAJECTORY METHODS

A. Description of the Potential Energy Function. The Ar−allyl potential is expressed as the sum of an intramolecular allyl potential and an interaction potential between the argon and the allyl. The intramolecular potential is based on a mathematical fit to 97418 electronic energies calculated at the CCSD(T)/aug-cc-pVTZ level, as described previously.[73,74] There are four stable isomers of C_3H_5, the conformations denoted GM (CH_2−CH−CH_2), LM1 (CH_3−C−CH_2), and LM2 (CH_3−CH−CH) and a triangular conformation LM3. Dissociation channels include H elimination to yield allene or propyne and methyl elimination to yield acetylene, either through a vinylidene intermediate from LM1 or directly from LM2.

The intermolecular Ar−allyl potential was approximated by a sum of pairwise potentials between the argon atom and each H or C atom of the allyl. This potential has also been described previously.[7] Briefly, each Ar−H or Ar−C potential is described as the sum of an exponential repulsion and an attractive potential, using functions described by Varandas and Rodrigues.[75] Parameters used in these functions are given by the IntPES2 column in Table 2 of ref 7, and contour plots of the potentials for argon interacting with the stable isomers are shown in Figure S1 of the Supporting Information. The parameters were found by fitting the potential equations to 286 points calculated at the MP2 level of theory with an aug-cc-pvtz (avtz) basis set using counterpoise correction.[77] The fit had an R^2 of 0.962 and an overall RMS error of 216 cm^{-1} (0.617 kcal/mol). For the attractive regions, the RMS error was 22 cm^{-1} (0.063 kcal/mol), while for energies around 1200 cm^{-1} (3.42 kcal/mol) the RMS error was 150 cm^{-1} (0.43 kcal/mol) and for energies around 8000 cm^{-1} (22.9 kcal/mol), it was about 650 cm^{-1} (1.9 kcal/mol).

B. Description of the Trajectory Methods. Classical trajectory calculations were performed as described previously[7,8] with the following modifications. The excitation energy above the allyl zero point energy was chosen to be 54974 cm^{-1} or 157.2 kcal/mol. This energy was chosen because it was used for both experiments[76] and trajectory calculations[73] on allyl alone and because it is high enough to access all of the observed dissociation channels. The collision energy was chosen to be 10 kcal/mol, which corresponds approximately to a temperature of 3332 K. Some previous trajectories at a collision energy of 2 kcal/mol (about 666 K) will also be described. In addition, trajectories were performed both with rotationless and rotating initial allyl radicals. In the latter case, the initial vibrational and rotational energies were determined microcanonically by assigning random velocities to each atom and scaling the total energy to be 54974 cm^{-1} (157.2 kcal/mol) above the zero-point energy of the GM isomer. The energies above the LM1, LM2, and LM3 isomers are, respectively, 47822, 46199, and 44663 cm^{-1}; these correspond to 136.7, 132.0, and 127.7 kcal/mol, respectively.

Trajectories were started with the allyl in one of the four stable isomers (GM, LM1, LM2, and LM3), and the initial orientation of the allyl with respect to the argon was varied by random rotation of the Euler angles. A small set of trajectories was run to determine the maximum impact parameter, b_{max}, using the time of the collision as a guide, as described previously.[7] This method eliminates much of the elastic spike near $\Delta J = 0$ and $\Delta E = 0$, although a small residual remains. The impact parameter for the main set of trajectories was then selected from values between 0 and b_{max} using a properly weighted Monte Carlo method.

The general strategy for computing the trajectories rests on the observation that the collision time (about 1 ps)[7] is considerably shorter than the time for reaction (typically 10−100 ps). Trajectories for the argon-ally collision were run until the argon atom and the allyl were separated by a distance of 15 au. The number of trajectories run was 29878 for the GM isomer, 26151 for the LM1 isomer, 21139 for the LM2 isomer, and 23717 for the LM3 isomer. Products of the collisional trajectories were characterized by an initial rotational level, J_i, a final rotational level, J_f, and change in total energy, ΔE. Further details are provided elsewhere.[8]

The classical trajectories are, of course, only an approximation to the quantum mechanical physics that governs the collisions. However, because the excitation energy and the collision energy are large, it is likely that the classical trajectories are a very good approximation for characterizing the angular momentum and energy transfer for this system.

IV. RESULTS

A. Collisional Energy Transfer for Argon with Allyl Isomers. The overall collisional energy transfer from a molecule starting in a state with energy and angular momentum ($E_i J_i$) to a state with energy and angular momentum ($E_f J_f$) can be described by the joint probability distribution, $P(J_i J_f \Delta E)$, where $\Delta E = E_f - E_i$. As described above, trajectories were run for C_3H_5 starting in each of the GM, LM1, LM2, and LM3 isomers with a total excitation energy above the GM zero point energy of 54974 cm^{-1} and encountering collisions with argon at a collision energy of 10 kcal/mol (3500 cm^{-1}). The results were tabulated according to $P(J_i J_f \Delta E)$, and the results were binned

dx.doi.org/10.1021/jp506202g | J. Phys. Chem. A 2014, 118, 7758−7775

typically with widths of $\Delta J_i = \Delta J_f = 25\hbar$ and $\Delta E = 350$ cm^{-1} (1.0 kcal/mol).

Figure 4 displays some typical results from the trajectories. The upper of the two contour plots shows the logarithm (base 10) of the joint probability distribution from the trajectories. The red dots in the top panel show the energy distribution from the trajectories summed over J_f, while the red dots in the next lower panel show the rotational distribution from the trajectories summed over ΔE. In each case, the blue curve is the prediction of the model with $a_{rot} = 1$, $a_{vib} = 1$, and $B_{ratio} = 0.8$. The contour predicted by the model is in the lowest panel. Several similar figures (Figures S9–S18) are included in the Supporting Information for GM with $J_i = 187.5$ and 237.5, for LM1, with $J_i = 137.5$, 187.5, and 237.5, for LM2 with $J_i = 137.5$, 187.5, and 237.5, and for LM3 with $J_i = 137.5$ and 187.5. It is clear from these results that the model captures, though not exactly, the principal variations in the joint probability distribution for collisions of argon with various isomers of allyl. In all cases, the model predictions are fairly good with $a_{rot} = 1$, $a_{vib} = 1$, and $B_{ratio} = 0.8$. The reason for choosing a value of B_{ratio} somewhat smaller than unity will be discussed in Discussion of the Assumptions.

A striking result of the trajectory calculations is that the energy transfer does not depend strongly on the identity of the starting isomer. The red dots in Figure 5 display in the top panel the joint probability distribution summed over J_f and, in the bottom panel, the join probability distribution summed over ΔE. Similarly, the blue, orange, and purple dots provide data for trajectories starting in LM1, LM2, and LM3, respectively. Gaussian binning has been used to smooth the trajectory data. It is evident that the energy transfer properties for the different isomers are similar. Equivalent results are found for $J_i = 87.5$, 187.5, 237.5, and 287.5, as shown in Figures S19–S22 of the Supporting Information.

It is perhaps surprising at first to find that there is so little effect of the starting isomer on the energy transfer properties. The argon interaction potentials, plotted in Figure S1 of the Supporting Information, show significant differences in the shape and magnitude of the potential energy as a function of isomer. Thus, the similarity in energy transfer outcomes is not due to a similarity in interaction potential. Nor is the similarity in energy transfer outcomes the result of collisional mixing of the isomers. The trajectory data show that, except for starting from LM3, over 96% of the configurations just following the collision were either the same as or closely related to the configuration before the collision.[8] For trajectories starting from LM3, breaking 1 C–C bond would give GM, so this also has a configuration following the collision that is "closely related" to the configuration before the collision. Thus, it is certainly not the case that there is complete scrambling between the configurations as a result of the collision. The reason for the similarity in energy transfer outcomes for the different isomers is because the orientationally averaged potentials are very similar, as discussed in Discussion of the Assumptions below.

A somewhat different comparison between the trajectories and the model can be made with allyl–argon collisions in which the allyl is initially in $J_i = 0$. For these trajectories, the collision energy was 2.0 kcal/mol. Figure 6 displays results in a fashion similar to that for Figure 4. It is surprising that even though the molecule is not rotating, and therefore not subject to rotational averaging, the model still predicts results that are in reasonable agreement with the trajectories.

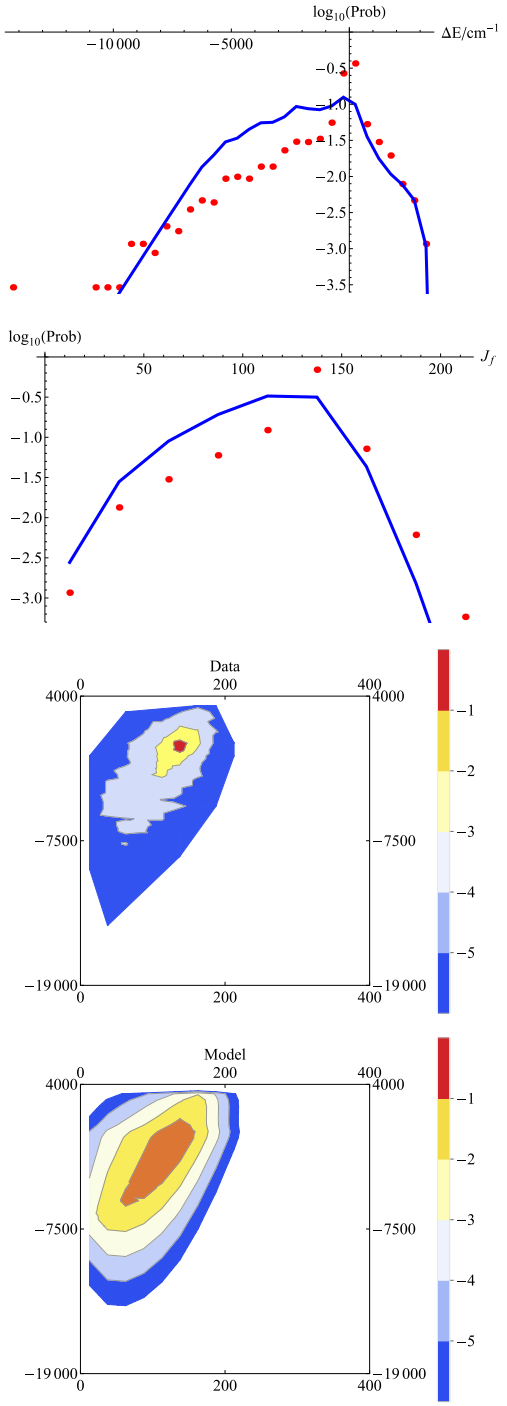

Figure 4. Joint probability distribution $P(J_f,\Delta E)$ for collisions of Ar with allyl starting in the GM configuration with $J_i = 137.5$ and for a collision energy of 10.0 kcal/mol. The contours in the bottom two panels represent a log10 scale of probability and are separated by 1.0 log units. The trajectory data contours are above those for the model results; the ordinate is ΔE/cm^{-1}, while the abscissa is J_f. The top panels give the trajectory results (red dots) and the model predictions (blue solid curve) for the energy distribution summed over J_f (top) and the rotational distribution summed over ΔE (bottom). The model parameters are $a_{rot} = 1$, $a_{vib} = 1$, and $B_{ratio} = 0.8$. Energies are in inverse centimeters, where 350 cm^{-1} = 1.00 kcal/mol.

V. DISCUSSION

A. Model for Collisional Energy Transfer in Highly Excited Molecules. *1. Discussion of the Assumptions.* We

dx.doi.org/10.1021/jp506202g | J. Phys. Chem. A 2014, 118, 7758–7775

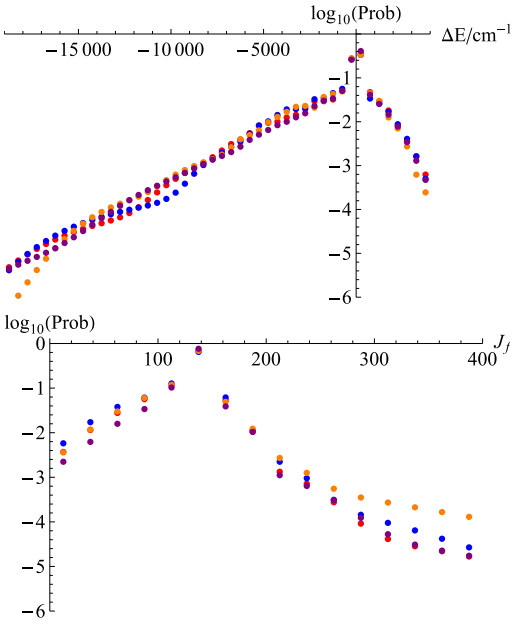

Figure 5. The joint probability distribution $P(J_f, \Delta E)$ for collisions of Ar and for J_i = 137.5 summed over J_f (top). The joint probability distribution $P(J_f\Delta E)$ for collisions of Ar and for J_i = 137.5 summed over ΔE (bottom). The starting isomers are GM (red), LM1 (blue), LM2 (orange), and LM3 (purple). In all cases, Gaussian binning has been used so as to be able to discern the differences between the isomers from the scatter. Energies are in inverse centimeters, where 350 cm^{-1} = 1.00 kcal/mol.

now examine the assumptions (a–e) made in developing the model of Model for Collisional Energy Transfer in Highly Excited Molecules. Of course, in the end analysis, whether the assumptions are reasonable will be determined by whether the model predicts the data from the trajectories, but it is important first to assess the limitations of and rationale for the assumptions.

(a) Essential features of the energy transfer are assumed to be described by an orientation-averaged potential $V(R)$. One surprising feature of the results is that the joint probability distributions for energy transfer are very similar for trajectories starting in GM, LM1, LM2, and LM3 (see Figure 5). The potential energy contours for the isomers, shown in Figure S1 of the Supporting Information, appear to be quite different from one another. However, as shown in Figure 7, the orientation-averaged potential energy curves are nearly identical. These orientation-averaged potentials were determined by taking the intermolecular potential function (typically a sum of pairwise interactions) and averaging it over Euler angles for each distance R from the center of mass. The fact that the energy transfer outcomes seem to correlate with the orientation-averaged potential energy curves suggests that the energy transfer depends only on this averaged potential energy and not on the more detailed shape of the potential. Of course, this conclusion may be specific to Ar–allyl or to situations where the orientationally averaged curves present the same atomic species to the incoming projectile. Further examples will be needed to test this assumption.

Table 1 shows numerically how similar the potential curves in Figure 7 are to one another. Each potential over the range of energy transfer interest can be represented to very high accuracy by a formula of the type

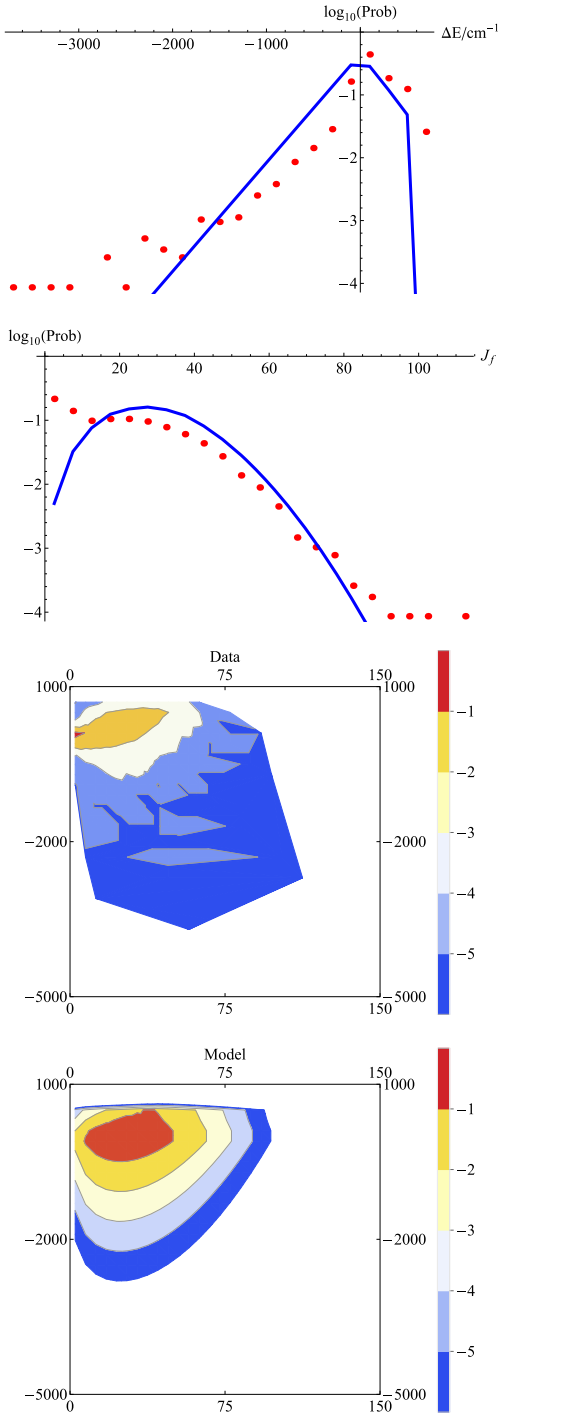

Figure 6. Joint probability distribution $P(J_f\Delta E)$ for collisions of Ar with allyl starting in the GM configuration with J_i = 0 and for a collision energy of 2.0 kcal/mol. The contours in the bottom two panels represent a $\log_{10}$ scale of probability and are separated by 1.0 units. The trajectory data contours are above those for the model result; the ordinate is $\Delta E/cm^{-1}$, while the abscissa is J_f. The top panels give the trajectory results (red dots) and the model predictions (blue solid curve) for the energy distribution summed over J_f (top panel) and the rotational distribution summed over ΔE (next panel). The model parameters are a_{rot} = 1, a_{vib} = 2, and B_{ratio} = 0.8. Energies are in inverse centimeters, where 350 cm^{-1} = 1.00 kcal/mol.

$$V(R) = (E_{rel} + \epsilon)\exp[-(R - r_{offset})/s_{range}] - \epsilon \quad (13)$$

dx.doi.org/10.1021/jp506202g | J. Phys. Chem. A 2014, 118, 7758–7775

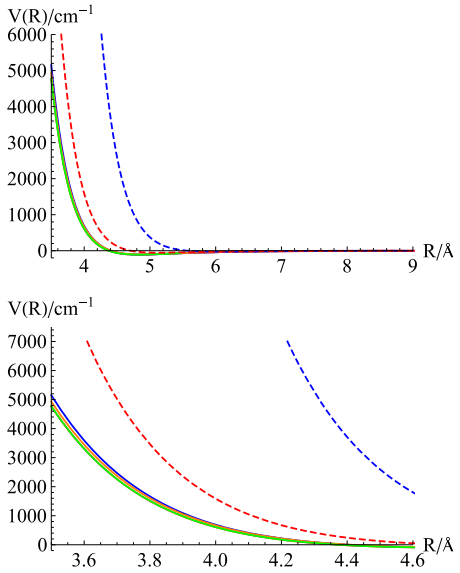

Figure 7. Orientationally averaged potential energy curves for argon−allyl isomers, where the distance is that to the center of mass of the isomer. The top panel shows a wide range of distance, while the bottom panel shows the region of interest for energy transfer. The blue curve is for trajectories starting in GM, the red for LM1, the orange for LM2, and the green for LM3. The red-dashed and blue-dashed curves are the pair potential for Ar−H and Ar−C used in the fit to the calculated intermolecular PES. Energies are in inverse centimeters, where 350 cm^{-1} = 1.00 kcal/mol.

Table 1. Characteristics of Orientation-Averaged Potentials and Spherically Averaged Rotational Constants Used in This Study[a]

potential	E_0	$r_{offset}(E_{rel})$	s_{range}	ϵ	B_{sph}
allyl GM	1.43×10^9	3.585 (3500)	0.280	230	0.4365
allyl LM1	1.63×10^9	3.639 (3500)	0.280	200	0.4020
allyl LM2	9.81×10^8	3.595 (3500)	0.288	220	0.4215
allyl LM3	1.23×10^9	3.584 (3500)	0.282	240	0.6080
ethane	3.98×10^8	–	0.283	100	0.9152
pyrazine	8.40×10^{15}	–	0.152	200	0.1529
methane	9.67×10^7	–	0.266	170	5.33
cis-HOCO	6.11×10^8	3.66 (350)	0.260	110	0.5444
trans-HOCO	2.21×10^9	3.69 (350)	0.239	85	0.5383

[a]The potential parameters are those in $V(R) = (E_0 + \epsilon) \exp[-R/s_{range}] - \epsilon$. For a fixed value of E_{rel}, these potentials can also be expressed as $V(R) = (E_{rel} + \epsilon) \exp[-(R - r_{offset})/s_{range}] - \epsilon$, where r_{offset} at the value of E_{rel} is given in the third column. Energies in the table are in wavenumbers (350 wavenumbers = 1 kcal/mol), while distances are in angstroms. All potentials are for the interaction with argon.

where E_{rel} is the energy of the turning point for $b = 0$, ϵ is an attractive well depth, r_{offset} is an offset defined as the solution to $V(r_{offset}) = E_{rel}$, and s_{range} is an exponential range parameter. Note that while this potential goes to $-\epsilon$ at large R, the only part of the potential that is used for the model is the potential between the position where $V(R) = E_{rel}$ and the position where $V(R) = 0$. It is clear when the potential is expressed this way that all of the argon−allyl potentials are characterized by similar offset and range parameters, as shown in columns 3 and 4 of Table 1. The range parameter s_{range} and the offset r_{offset} are the only parameters that appear directly in the model. The vibrational energy transfer is exponentially sensitive to s_{range}, while the rotational energy transfer depends strongly on r_{offset}. Orientation-averaged potentials for argon with ethane, pyrazine, methane, and *cis*- and *trans*-HOCO will be discussed in Model Predictions for Other Systems.

At first it may seem strange that a model based on only the orientation averaged potential can predict anything quantitative concerning the energy transfer. However, nearly all trajectory calculations and experiments are carried out with random orientations of the target molecule relative to the direction of the incoming atom. Thus, even in the case where the target molecule is not rotating, the experiment or trajectory performs orientation averaging. The assumption that the essential features of the energy transfer are described by an orientation-averaged potential $V(R)$ amounts to an assumption that the energy transfer changes fairly smoothly with orientation (i.e., that there are no "sweet spots" where energy transfer is highly efficient). Mathematically, this amounts to the assumption that the average of the energy transfer as a function of orientation is nearly equal to the energy transfer as a function of the average orientation. Of course, this assumption also means that, to the extent that they depend on special features of the potential, the model will fail to predict any "highly efficient energy transfer" encounters, such as those that have been found for argon−allyl collisions,[8] for collisions of CS_2 with small molecules,[78] and other systems.

(b) Rotational energy for a state J is assumed to be characterized by $B_{sph}\,J(J+1)$, where B_{sph} is the spherically averaged rotational constant for the molecule. The justification for taking the spherically averaged rotational constant follows directly from treating the target molecule as a spherical object. This spherical approximation allows the separation of vibrational and rotational energy transfer in the soft-sphere/line-of-centers model. In order for the rotational transfer to be consistent with this model, the rotational constant needs to be that for a spherical target molecule. However, some corrections may be necessary.

Because the spherically averaged rotational constant is calculated based on the ground-state equilibrium structure of the molecule, it may not be appropriate for highly excited vibrational levels, where the atoms are, on average, further from the center of mass both because of centrifugal distortion and because of the vibration−rotation interaction. Centrifugal distortion reduces the term values of rotation states, as described by the formula $F(J) = J(J+1)B_e - DJ^2(J+1)^2$. Here, B_e is the rotational constant based on the equilibrium configuration and D is a centrifugal distortion constant related to the vibrational frequency by $D = 4B_e^3/\omega^2$. The centrifugal distortion reduces the effective rotational constant. However, the effect is small. For ω = 900 cm^{-1}, B_{rot} = 0.4365, and J = 137, the reduction is about 2%.

A much larger reduction comes from the fact that the average stretch distance in a vibrationally excited molecule is larger than in a ground-state one. The effect is described spectroscopically by the formula $B_0 = B_e - (1/2)\Sigma_r \alpha_r^B$, where the sum is over the 3N-6 (3N-5) vibrational modes of the molecule with N equal to the number of atoms.[79] For an excited molecule in a particular mode, the reduction is given by $B_v = B_e - \alpha(v + 1/2)$. Table 3 of ref 79 lists experimental and calculated values of $\Sigma_r \alpha_r^B$ for some simple molecules. Assuming excitation of 20000−50000 cm^{-1} and a vibrational frequency of 2000 cm^{-1}, we would have values of v in the range from 10 to 25. An average value of $(\Sigma_r \alpha_r^B)/B_e$ for several molecules listed is about 0.018, so in the range of excitation the correction could amount to a reduction

dx.doi.org/10.1021/jp506202g | J. Phys. Chem. A 2014, 118, 7758−7775

in the rotational constant of 18−45%. Thus, it is reasonable to assume $B_{rot} = B_{ratio}B_{sph}$, where B_{ratio} could be smaller than unity.

Confirmation of this general conjecture comes from an examination of the trajectory data. For example, the trajectories for allyl in the GM isomer with an excitation energy of 54974 cm^{-1} (157.2 kcal/mol) show configurations that, when averaged over 25 trajectories of roughly 2000 positional outputs per trajectory, give a spherical rotational constant of 0.402 with a standard deviation of 0.043. When compared to the equilibrium spherical rotational constant of 0.4365 for this isomer, B_{ratio} is somewhere between 0.81 and 1.03 (to one standard deviation). Similar results are found for other isomers,[8] where excited values of B_{sph} and its standard deviation are given by LM1: {0.370,0.043}; LM2: {0.393,0.047}; and LM3: {0.477,0.086} as compared to equilibrium values of 0.401, 0.424, and 0.607, respectively.

(c) Vibrational energy can be transferred to/from the target molecule during the collision in any amount [i.e., the vibrational frequency distribution of the molecule (its density of vibrational states) is smooth as a function of frequency]. If the target molecule is treated classically then the vibrations are not quantized and this assumption is automatically met. However, if the target molecule is treated quantum mechanically then at least at low excitation energies, the frequencies are constrained to be multiples of the fundamental frequencies. The original Landau−Teller model, based on perturbation theory, treats the vibrations of the target molecule (a diatomic) quantum mechanically. In extending the Landau−Teller model to a target molecule of many atoms at very high excitation, we make the assumption that the molecule has vibrations at all frequencies (it is in the quasicontinuum) and that, therefore, any amount of vibration can be transferred between the atom and the target consistent with conservation of energy. For very highly excited polyatomic molecules, this seems a reasonable assumption. There will be some amplitude of vibration at every frequency, so that energy transfer, while perhaps depending linearly on the density of vibrational levels, should still vary exponentially with $|\Delta E_{vib}|$. Of course, as the excitation energy for a polyatomic molecule decreases, its frequency spectrum will become more "lumpy" and at the lowest energies, the lumps will correspond to the frequencies of the normal modes. In such situations, it may not be possible to exchange an arbitrary $|\Delta E_{vib}|$. In principle, the inclusion of the density of states ratio in eq 1 helps to correct for the "lumpiness", but most models for the variation of the density of states with energy are quite smooth.

An interesting feature of the model is that, while it depends strongly on the intermolecular potential, the only place where the intramolecular potential has a substantial influence is in the variation of the density of states with energy. To the extent that the model is predictive, this observation suggests that most improvements can be made by treating the intermolecular potential more realistically.

(d) Energy transfer does not occur if the energy evaluated along the line of centers is negative. This assumption seems intuitive but should be examined in more detail. The collision time, τ_c, increases rapidly as the impact parameter goes from 0 to R_0, at which point the energy along the line of centers goes to zero. At larger b, the energy along the line of centers is negative. At these large impact parameters, the relative velocity between the atom and target molecule is essentially unchanged. The atom may feel a force directed toward the target molecule due to the attractive potential, but the attractive energy along the line of centers is not enough to overcome the attractive well. As a result, there is little deflection, so that $L_f \approx L_i$, and J_f must then be nearly the same as J_i. Thus, there is little or no rotational energy transfer. The vibrational energy transfer is also small because the force against the molecule is nearly zero and is exerted very slowly (i.e., adiabatically). Such collisions (with $b > R_0$) can thus contribute mostly to the elastic scattering, where $\Delta E_{vib} = 0$ and $J_f = J_i$. The consequence of this assumption is that the only part of the potential that matters for energy transfer is between $R = r_{offset}$ and $R = R_0$.

One assumption of a line-of-centers model can be examined by plotting the actual turning points from the trajectories and comparing them to the prediction of turning points for the orientation-averaged potential. Figure 8 shows the results for

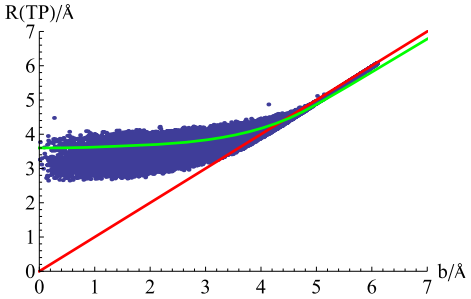

Figure 8. Turning points for trajectories (blue dots) and those predicted by the orientation-averaged potential function (green line). The red line plots $R(TP) = b$.

trajectories starting in the GM isomer. The green line predicted from the orientation-averaged potential appears to give a sensible interpolation of the trajectory points in blue. Recall that the orientation-averaged potential is fit by a function of the form $V(R) = (E_{rel} + \epsilon) \exp[-(R - r_{offset})] - \epsilon$, which is highly accurate for the region between $R = r_{offset}$ and $R = R_0$. However, this potential remains negative at large R, and this is the reason that the predicted turning points in green do not return to the line $R(TP) = b$ at large R. We note that while the green line gives a sensible interpolation to the trajectory calculations, the wide variation in turning points indicates that orientational effects may play a significant role and should be addressed in any improvement of the model.

Looking in more detail at Figure 8, we see that there are many trajectories that penetrate well into the sphere, describing the rotationally averaged potential for the GM isomer, which has $r_{offset} = 3.6$ Å. How serious is this problem, and will it cause a breakdown of the model? The answer is that the assumptions of the model depend more on the potential at the surface of the molecule's shape rather than on having the shape be a sphere. The range parameter, (s_{range}, for an exponential potential) is the most important parameter for the vibrational transfer, while the parameter r_{offset} is the most important parameter for the rotational transfer. The advantage of having approximated the target molecule by a sphere is that the two motions are effectively separated, with P_{vib} depending on E_{loc} and P_{rot} depending on $E_{perploc}$. For molecules with pockets or protuberances, the vibrational and rotational excitation/de-excitation become mixed, with E_{loc} contributing to rotation and $E_{perploc}$ contributing to vibration. However, the approximation of spherical symmetry is still one that captures the essential physics of the problem. As can be seen from the results for trajectories starting in $J = 0$ from the GM geometry with E_{rel} =

dx.doi.org/10.1021/jp506202g | J. Phys. Chem. A 2014, 118, 7758−7775

700 cm^{-1} (2.0 kcal/mol) in Figure 6, even when the target molecule is not rotating at all, the model is still in reasonable agreement with the data because the potential that the incoming atom feels is, on average, the orientation-averaged potential.

(e) Rotational energy transfer is governed by a simple phase-space model and is caused by a change in the orbital angular momentum as evaluated using the velocity along a line perpendicular to the line of centers. The phase space model[71,72] is a well-established approach that has yielded reasonable results and good insight. While more detailed theories are available,[65−70] the phase-space approach has the virtue that it is easy to evaluate and has the correct behavior. As shown in the Appendix of the Supporting Information, it predicts soft exponential falloff for both positive and negative ΔE_{rot}, followed by much more rapid exponential falloff on each side when conservation of angular momentum limits the range of impact parameters that can contribute to the energy transfer. The comparison of the model with the trajectory results on argon−allyl shown in Figure 4 and Figures S9−S18 of the Supporting Information provides fairly convincing evidence that the basic approach is correct.

Models of physical phenomena are important for at least two reasons: they predict the outcome of experiments, and they allow one to see how the fundamental physics, often simple, accounts for more complex behavior. Comparison of the prediction of the model with the outcome of trajectory calculations on argon−allyl has been examined in Results. Comparison to the results of other calculations will be examined in Model Predictions for Other Systems. Before moving to these comparisons, we briefly summarize some of the physical insights that the model provides.

2. Insights from the Model. An observation from the discussion of assumption (a) in Discussion of the Assumptions is that the orientation-averaged potentials for different isomers are very similar. This similarity may be the cause of the similar energy transfer results. The repulsive part of the potential between the potential values of E_{rel} and 0 are all nearly the same, as characterized by similar s_{range} parameters. Furthermore, the orientation-averaged potential is similar both to the argon−H potential and to the argon−C potential in the pairwise sum that describes the intermolecular potential. Support for the importance of the argon−H potential comes from the trajectory studies. The fraction of collisions that have their minimum turning point closest to an H atom is 94%, 91%, 87%, and 94% for trajectories starting in the GM, LM1, LM2, and LM3 isomers, respectively. Finally, while the energy transfer no doubt also depends on the asymmetry of the molecule and the density of states, the first of these is similar for the isomers and the second is identical, at least in the commonly used formula describing how the density of states varies with energy.[35]

This observation invites some speculation about other hydrocarbon systems. In typical hydrocarbons, the hydrogen atoms are farther from the center of mass than the carbon, oxygen, nitrogen, etc. When the intermolecular potential between the hydrocarbon and the atom is orientation averaged, it will be the hydrogens that are on the outside. One might then speculate that the orientation-averaged intermolecular potential for all hydrocarbons will simply be a shifted pair potential between the incoming atom and a bonded hydrogen atom; all hydrocarbon potentials for the same incoming atom might have similar range parameters, s_{range}. The difference, then, between different hydrocarbons would be in the offset shift. In this view, the only functions of the heavier atoms are (a) to act as a scaffold to hold the hydrogens at some distance shifted by r_{offset} from the center of mass and (b) to determine the reduced mass and rotational constant. In the model for energy transfer, the offset affects the rotational energy transfer but not the vibrational energy transfer.

Several other insights can be obtained by examining how the joint probability distribution varies with the parameters E_{rel}, s_{srange}, B_{sph}, and μ, as discussed in Appendix SII of the Supporting Information.

B. Model Predictions for Other Systems. *1. Comparison of Model Predictions with Argon-Ethane and Argon-Pyrazine Data.* Barker and Weston, Jr.[35] used quasi-classical trajectory calculations to study the joint probability distributions for energy transfer in Ar−pyrazine and Ar−ethane collisions. A goal of their paper was to develop a flexible formula to describe the joint probability distribution. The collisional aspect of the trajectories was calculated at the canonical level of averaging, typically with T_{trans} = 300 K, although results at other temperatures were also reported. The target molecule was treated at the microcanonical level. The argon−ethane and argon−pyrazine interactions were modeled by an exponential-6 or Lennard-Jones pairwise potential, and the intramolecular potentials were based on a classical model chosen to match experimental vibrational frequencies. Interesting data were obtained from the trajectories and interpreted with an original and useful formula.

The major conclusion of the Barker and Weston, Jr. paper was that the final rotational energy distribution is not independent of the initial distribution, so that a two-dimensional joint energy transfer description is required. The authors proposed that the form of the joint probability distribution should follow a particular, flexible formula, $P(E,J;E',J') = \Sigma_{i=1}^{2} C_i f_{Ti} \exp(-f_{ai})$, where T_i is a temperature characterizing the collision, C_i are adjustable amplitudes, and the functions f_i are defined in the reference and characterized by four parameters for each value of i. The summation over two functions allows one function to account for the elastic peak.

The simple physical model that we have developed predicts the results of the Barker and Weston trajectories with reasonable accuracy. Fits of their phenomenological formula to the data are provided in Supporting Information to their article.[35] We used their intermolecular potential parameters to derive orientation-averaged potentials, whose parameters for argon-ethane and argon-pyrazine are listed in Table 1. Equation 12 was used with integration over E_{rel} using a thermal distribution at 300 K.

Figure 9 shows a result for argon with ethane. The spherically averaged rotational constant for ethane is 0.9512 cm^{-1}, and the model used a_{rot} = 4, a_{vib} = 3, and B_{ratio} =0.7. Calculations were performed for conditions appropriate to Figures 4a/6a, 4c/6c/ and 4e/6e of the Barker and Weston Jr. paper.[35] Figure 9 is for J_i = 37.47.

Barker and Weston Jr. also reported results for the collisions of argon with pyrazine.[35] Figure 10 shows the prediction of our model along with their results, as represented by their 10-parameter formula. We used their potential functions to calculate the orientation-averaged potential listed in Table 1. The spherically averaged rotational constant is 0.1529 cm^{-1}. Figure 10 is for conditions relevant to Figures 3c/5c of ref 35. Parameters used for the model prediction were a_{rot} = 2, a_{vib} = 8, and B_{ratio} = 0.9.

dx.doi.org/10.1021/jp506202g | J. Phys. Chem. A 2014, 118, 7758−7775

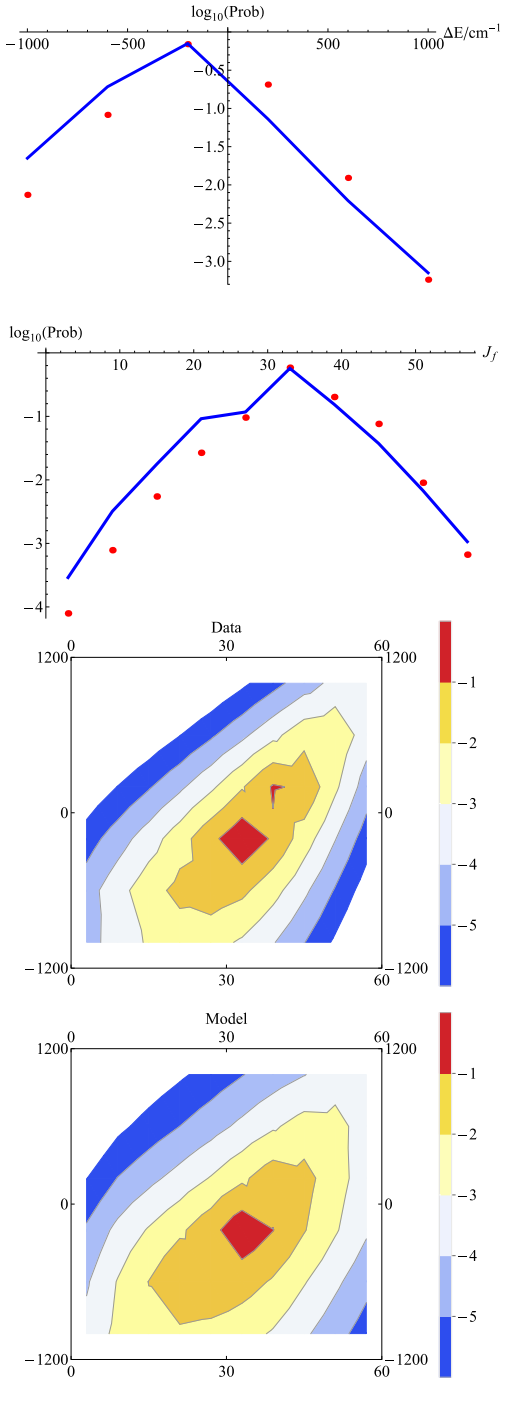

Figure 9. Joint probability distribution $P(J_f,\Delta E)$ for collisions of Ar with ethane starting with J_i = 37.47 and for a translational temperature of 300 K. The contours in the bottom two panels represent a $\log_{10}$ scale of probability and are separated by 1.0 log units. The contours for the trajectory data are above those for the model results; the ordinate is $\Delta E/\mathrm{cm}^{-1}$, while the abscissa is J_f. The top panels give the trajectory results from ref 35 (red dots) and the model predictions (blue solid curve) for the energy distribution summed over J_f (top) and the rotational distribution summed over ΔE (bottom). The model parameters are a_{rot} = 4, a_{vib} = 3, and B_{ratio} = 0.7. Energies are in inverse centimeters, where 350 cm^{-1} = 1.00 kcal/mol.

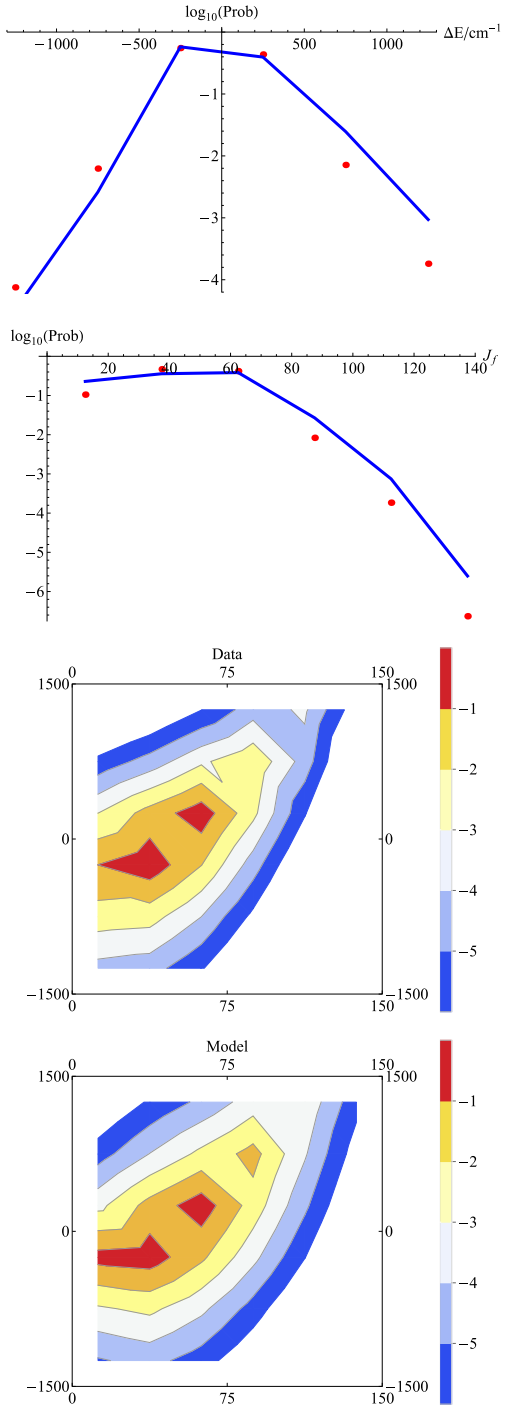

Figure 10. Joint probability distribution $P(J_f,\Delta E)$ for collisions of Ar with pyrazine starting with J_i = 42.274 and for a translational temperature of 300 K. The contours in the bottom two panels represent a $\log_{10}$ scale of probability and are separated by 1.0 log units. The contours for the trajectory data are above those for the model results; the ordinate is $\Delta E/\mathrm{cm}^{-1}$, while the abscissa is J_f. The top panels give the trajectory results from ref 35 (red dots) and the model predictions (blue solid curve) for the energy distribution summed over J_f (top) and the rotational distribution summed over ΔE (bottom). The model parameters are a_{rot} = 2, a_{vib} = 8, and B_{ratio} = 0.9. Energies are in inverse centimeters, where 350 cm^{-1} = 1.00 kcal/mol.

It is clear from Figures 9 and 10 that there is very good agreement between the prediction of (12) and the results reported by Barker and Weston, Jr. for argon with ethane or pyrazine.[35] Two other figures for argon−ethane, with J_i = 18.735 and J_i = 9.376, and two other figures for argon−pyrazine, with J_i = 82.659 and J_i = 22.637, are shown in Figures S23−S26 of the Supporting Information. The agreement is

dx.doi.org/10.1021/jp506202g | J. Phys. Chem. A 2014, 118, 7758−7775

similar to that shown in Figures 9 and 10. We conclude that the model works well for argon−ethane and argon−pyrazine. We also note that the potential parameter s_{range} for ethane (0.283) is very similar to that for the allyl isomers (0.280−0.288). The value of s_{range} for pyrazine (0.159) is somewhat smaller than those where the argon−H interaction is dominant.

2. Comparison of Model Predictions with Argon-HOCO Data. We have recently reported a benchmark potential for argon−HOCO and compared it with a pairwise potential to see how predictions of the average energy transfer for the down collisions might depend on potential.[41] The trajectory data that we obtained for this system included the joint probability distribution, although this distribution was not reported in the communication. The pairwise potential, called P-18, did not predict an average down energy in close agreement with the benchmark potential (the prediction was about 30% too low), but it is nonetheless interesting to see if the results of our model are consistent with the results from the trajectories using the same potential. For the current purposes, we augmented the 7000 trajectories reported[41] with another 18000. We then determined the orientation-averaged potentials for argon with both *cis*-HOCO and *trans*-HOCO (see Table 1). The spherically averaged rotational constants are both close to 0.54 cm^{-1}. Figure 11 shows the results for argon with *cis*-HOCO. The collision energy is 350 cm^{-1} (1.0 kcal/mol), and J_i = 0. For the model, α_{rot} = 1, α_{vib} = 14, and B_{ratio} = 0.8.

Similar agreement was found for argon with *trans*-HOCO, as shown in Figure S27 of the Supporting Information. The average energy change for those trajectory collisions that produced $\Delta E \leq 0$ was −27.3 cm^{-1} based on the 25000 argon−HOCO trajectories. For the model calculation, from the joint probability distribution described in Figure 11, we obtained −28.7 cm^{-1} (0.082 kcal/mol) for *cis*-HOCO and −31.2 cm^{-1} (0.089 kcal/mol) for *trans*-HOCO. Thus, provided that there is enough data (e.g., a joint probability distribution) to determine the adjustable parameters, it appears that the model can accurately predict average energy changes.

3. Comparison of Model Predictions with Argon-Methane Data. Jasper and Miller have reported the results of trajectory calculations for excited methane in collision with several different atoms and with methane itself.[32−34] In particular, they report as a function of temperature two highly averaged energy change values for collisions of argon with excited methane,[33] the average energy lost in collisions that have $\Delta E < 0$, denoted $<\Delta E_d>$, and the rms average energy transferred, $<\Delta E^2>^{1/2}$. The intermolecular potential they used was taken from the paper by Alexander and Troya.[80] The orientation-average of this potential is listed in Table 1 along with the value of B_{sph}, which in this case is equal to the normal rotational constant.

Calculation of the averaged quantities requires averaging the joint probability distribution not only over impact parameter but also over relative energy E_{rel} and initial rotational level J_i. Figure 12 shows the results of these calculations in red and green along with the results of their trajectory studies in blue. The model predicts values for both sets of parameters that are higher than values from the trajectories, particularly at high temperature, and the slopes with temperature are somewhat higher than those for the trajectories as well. One might have expected better agreement for this system, since methane is the only molecule we have studied that actually is spherical. Further study and comparison are certainly warranted.

4. Generalizations about Hydrocarbons. One insight from the model is that hydrocarbons might have similar energy transfer properties when scaled for r_{offset}. An analysis of the trajectories for argon with allyl isomers[8] shows that at the

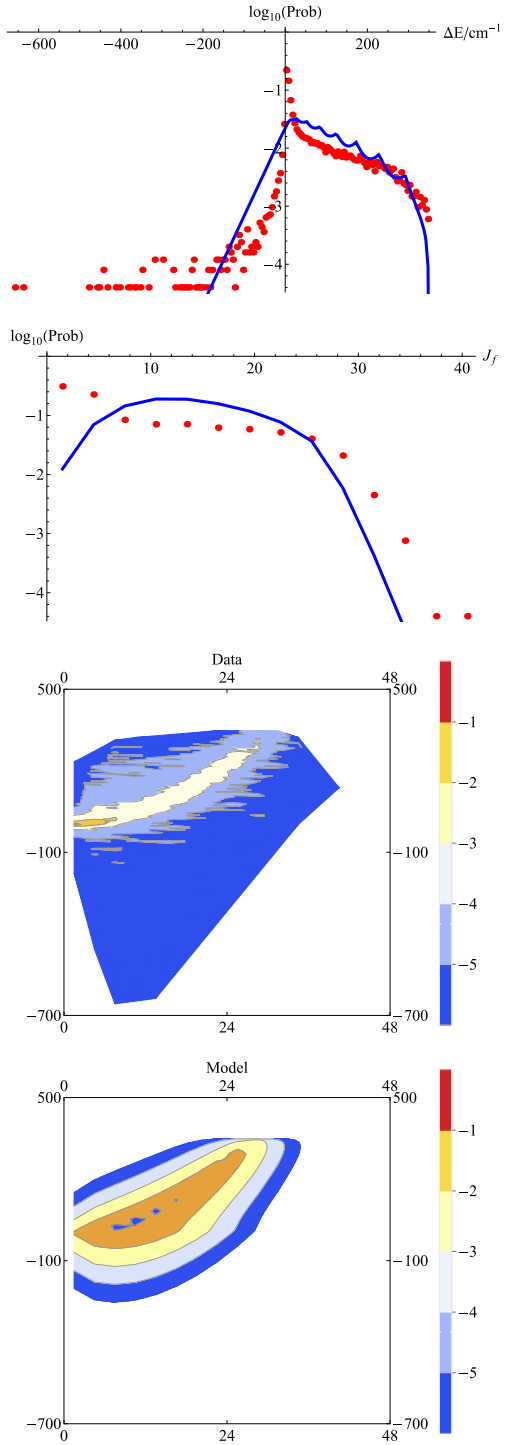

Figure 11. Joint probability distribution $P(J_f,\Delta E)$ for collisions of Ar with *cis*-HOCO starting with J_i = 0 and for a translational energy of 350 cm^{-1} (1.0 kcal/mol). The contours in the bottom two panels represent a $\log_{10}$ scale of probability and are separated by 1.0 units. The contours for the trajectory data are above those for the model results; the ordinate is $\Delta E/cm^{-1}$, while the abscissa is J_f. The top panels give the trajectory results (red dots) and the model predictions (blue solid curve) for the energy distribution summed over J_f (top) and the rotational distribution summed over ΔE (bottom). The model parameters were a_{rot} = 1, a_{vib} = 14, and B_{ratio} = 0.8. Energies are in inverse centimeters, where 350 cm^{-1} = 1.00 kcal/mol.

dx.doi.org/10.1021/jp506202g | J. Phys. Chem. A 2014, 118, 7758−7775

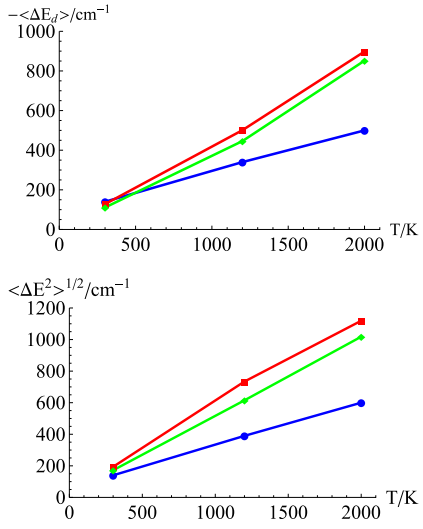

Figure 12. Comparison of average energy down (top) and rms energy transfer (bottom) between the results of trajectory calculations (blue) by Jasper and Miller on argon with methane[33] and the predictions of the model using parameters a_{rot} = 8, a_{vib} = 10, and B_{ratio} = 0.8 (red) or a_{rot} = 10, a_{vib} = 15, B_{ratio} = 0.8 (green). Energies are in inverse centimeters, where 350 cm^{-1} = 1.00 kcal/mol.

turning point the closest atom is a hydrogen 94% of the time for the GM isomer, 94% for LM1, 87% for LM2, and 94% for LM3. Thus, the incoming argon atom nearly always experiences an argon−hydrogen potential, and these should have similar potential parameters. Examination of Table 1 shows that the s_{range} parameters for the hydrocarbons listed are from 0.280 to 0.288 for allyl, and from 0.152 to 0.288 among all the systems studied. When one looks in more detail at the pairwise potentials that go into the orientation averaged potentials, it is clear that when there are several hydrogen atoms on the perimeter of the molecule, s_{range} is close to 0.28 and similar to the pair potential for argon and a bonded hydrogen. Of course, a molecule such as HOCO is only barely a hydrocarbon. In HOCO, as well as in pyrazine, the offset of the pairwise potentials of argon with O, C, or N are comparable to the offset with H, whereas in allyl and ethane, the argon−H offset is considerably larger than the offset for the argon−C potential. While it remains to be further verified, it does appear that when hydrogens are prominent in the periphery of the hydrocarbon, the energy transfer properties can be determined approximately from the radius of the spherically averaged hydrocarbon using a value for s_{range} of about 0.28. A remaining question, of course, is why the parameter a_{vib} is near unity for allyl and between 3 and 8 for ethane. More examples for comparison will be needed, as well as better methods for estimating a_{vib} for realistic systems.

VI. CONCLUSIONS

A soft-sphere/line-of-centers model has been developed for collisional energy transfer in highly excited molecules. Vibrational transfer is treated using an adiabaticity approach, while rotational transfer is treated using phase-space theory. The model, even with no adjustable parameters, correctly predicts most features of the energy transfer observed in trajectories for argon with allyl isomers performed using a realistic potential energy surface. Extension of the model with three adjustable parameters allows good fits to the results of many other trajectory studies, including those of argon with ethane and pyrazine[35] and argon with HOCO.[41] The agreement with a trajectory study of argon with methane[33] is somewhat less satisfactory and should be investigated further.

There are several limitations to the model, many of which have been discussed in the main part of the paper. To make these clear, we briefly summarize the limitations here. The model depends on the assumptions listed in Development of the Model and discussed in Discussion of the Assumptions. Many of these assumptions should be tested against new trajectory or experimental results. It is clear that the reliance on an orientation-averaged potential is a simplification, but how the model will succeed when the degree of asymmetry is large remains to be determined. The wide variation in turning points in Figure 8 suggests that orientational effects might be important. On the other hand, the agreement of the model predictions with the trajectory results for allyl suggest that, in this case, either they are not important or they average out. More examples will be needed to understand this result. The vibrational relaxation depends on the Landau−Teller formula, which while getting the basic physics right is itself a simplification. The rotational relaxation depends on phase-space theory and, in the original version (with a_{rot} = 1), is based on a "hard collision" assumption. Larger values of a_{rot} "soften" the collision, but it is not clear how to determine the correct value of a_{rot}. Furthermore, because the potential is assumed to be spherically symmetric, there is no rotational excitation from the motion along the line of centers; vibrational excitation and rotational excitation are separate processes. In asymmetric molecules, rotational excitation from motion along the line of centers is clearly important. Finally, although the excitation and collision energies in the problems considered are quite high, both the model and the trajectories to which it is compared are primarily classical. To the extent that quantum mechanics differs from classical mechanics, neither the trajectories nor the model will be correct. The model is clearly a first step toward more realistic models. The limitations must be kept in mind, but they also serve as a guide as to how the model might be improved.

One improvement would be a method for estimating the values of the three adjustable parameters for real systems. The value of B_{ratio} should usually be less than unity, for reasons discussed above, but will this hold for other systems? The values of a_{rot} and a_{vib} seem usually to be in the range from 1 to 10; values higher than unity indicate that the rotational or vibrational energy transfer is correspondingly less efficient than assumed in the original model. In the case of vibration, the decrease in efficiency is likely to be a result of collisions that provide less energy along the line of centers. In the case of rotation, it is likely that the collision does not have its turning point as far from the center of mass as assumed in the model. Further, while they are separately calculated quantities in the model system, in realistic systems, the mixing of vibrational and rotational energy transfer is probably ubiquitous. For example, when vibrational excitation decreases substantially, the atom will leave with more velocity than it had to begin with. In the realistic case, some rotation is caused by the velocity change normal to the potential surface, so the vibrational de-excitation will increase the probability of rotational change. Extending the model to such situations of mixed vibrational/rotational transfer might provide insights into parameter determination.

One approach might be to use the real intermolecular potential rather than the orientation-averaged one, to calculate as a function of b and orientation the values of d_{force}/v_{loc} and ΔJ_{max} and to average these values over b and orientation. Of

dx.doi.org/10.1021/jp506202g | J. Phys. Chem. A 2014, 118, 7758−7775

necessity, this approach, now underway, would involve evaluating a competition between vibrational energy exchange and angular momentum exchange, a feature that is lacking in the current model. While this approach seems reasonable, the fact that the excited molecules have a fluxional and essentially unknown structure means that many details of the interaction will still be predicted incorrectly. On the other hand, the fact that the model is reasonably successful while depending on the intramolecular potential only through the density of states gives hope that this approach might work.

Other areas for future work would be improved estimation of the density of states function, perhaps by direct count, integration of the model predictions with the master equation approach,[6] and integration of the model with the hard ellipse model for rotational energy transfer.[70,81,82]

There is great value in performing trajectory studies of collisional energy transfer in highly excited molecules, particularly at the microcanonical level. Such studies both stimulate model development and allow detailed examination of conjectures that arise in evaluating the models.

■ ASSOCIATED CONTENT

Supporting Information

Contour plots; comparison between results of numerical integration of eq (1) and use of the approximate eq (12) for allyl; joint probability distribution; appendix SI, details of the Pvib and Prot Models; and appendix SII, Anatomy of the joint probability distribution and its dependence on model parameters. This material is available free of charge via the Internet at http://pubs.acs.org.

■ AUTHOR INFORMATION

Corresponding Author

*E-mail: paul.houston@cos.gatech.edu.

Notes

The authors declare no competing financial interest.

■ ACKNOWLEDGMENTS

The authors thank J. Barker and R. Weston, Jr. for providing computer programs for the formulae listed in their paper[35] and J. Barker and G. Schatz for useful discussions. This material is based upon work supported by the U.S. Department of Energy, Office of Science, Office of Basic Energy Sciences under Award DE-FG02-97ER14782.

■ REFERENCES

(1) Lindemann, F. A. Discussion on the Radiation Theory of Chemical Action. *Trans. Faraday Soc.* **1922**, *17*, 598−599.
(2) Christiansen, J. A.; Kramers, H. A. Velocity of Chemical Reactions. *Z. Phys. Chem.* **1923**, *104*, 451−471.
(3) Houston, P. L. Vector Correlations in Photodissociation Dynamics. *J. Phys. Chem.* **1987**, *91*, 5388−5397.
(4) Houston, P. L. Correlated Photochemistry: The Legacy of Johann Christian Doppler. *Acc. Chem. Res.* **1989**, *22*, 309−14.
(5) *Molecular Photodissociation Dynamics*; Ashfold, M. N. R., Baggott, J. E., Eds.; Royal Society of Chemistry: London, 1987.
(6) Barker, J. R.; Golden, D. M. Master Equation Analysis of Pressure-Dependent Atmospheric Reactions. *Chem. Rev.* **2003**, *103*, 4577−4591.
(7) Conte, R.; Houston, P. L.; Bowman, J. M. Classical Trajectory Study of Energy Transfer in Collisions of Highly Excited Allyl Radical with Argon. *J. Phys. Chem. A* **2013**, *117*, 14028−14041.
(8) Conte, R.; Houston, P. L.; Bowman, J. M. Trajectory Study of Energy Transfer and Unimolecular Dissociation of Highly Excited Allyl with Argon. *J. Phys. Chem. A* **2014**, DOI: 10.1021/jp5062013.
(9) Tardy, D. C. Competitive Stabilization: New Method for Obtaining Vibrational Energy-Transfer Probabilities in Chemical Activation Systems. *Abstr. Pap., Jt. Conf.-Chem. Inst. Can. Am. Chem. Soc.* **1977**, *173* (MAR20), 175−175.
(10) Smith, G. P.; Barker, J. R. Energy-Transfer Rates for Vibrationally Excited Gas-phase Azulene in the Electronic Ground State. *Chem. Phys. Lett.* **1981**, *78*, 253−258.
(11) Barker, J. R. Direct Measurements of Energy-Transfer Involving Large Molecules in the Electronic Ground-State. *J. Phys. Chem.* **1984**, *88*, 11−18.
(12) Barker, J. R.; Toselli, B. M. Infrared-Emission Studies of the Vibrational Deactivation of Benzene Derivatives. *Int. Rev. Phys. Chem.* **1993**, *12*, 305−338.
(13) Hippler, H.; Lindemann, L.; Troe, J. Collisional Energy Transfer of Vibrationally Highly Excited Molecules. V. UV Absorption Study of Azulene. *J. Chem. Phys.* **1985**, *83*, 3906−3912.
(14) Hippler, H.; Troe, J.; Wendelken, H. J. Direct Observation of Collisional Deactivation of Highly Excited Toluene. *Chem. Phys. Lett.* **1981**, *84* (2), 257−259.
(15) Hippler, H.; Troe, J. Recent Direct Studies of Collisional Energy Transfer on Vibrationally Excited Molecules in the Electronic Ground State. In *Advances in Gas-Phase Photochemistry and Kinetics: Bimolecular Collisions*; Ashfold, M. N. R., Baggott, J. E., Eds.; The Royal Society of Chemistry: London, 1989; p 209.
(16) Löhmannsröben, H. L.; Luther, K. Selective Multiphoton Ionization in Dense Manifolds of Vibrational States. *Chem. Phys. Lett.* **1988**, *144*, 473−478.
(17) Mullin, A. S.; Michaels, C. A.; Flynn, G. W. Molecular Supercollisions: Evidence for Large Energy Transfer in the Collisional Relaxation of Highly Vibrationally Excited Pyrazine by CO_2. *J. Chem. Phys.* **1995**, *102*, 6032−6045.
(18) Weston, R. E., Jr.; Flynn, G. W. Relaxation of Molecules with Chemically Significant Amounts of Vibrational Energy: The Dawn of the Quantum State Resolved Era. *Annu. Rev. Phys. Chem.* **1992**, *43*, 559−590.
(19) Oref, I.; Tardy, D. C. Energy Transfer in Highly Excited Polyatomic Molecules. *Chem. Rev.* **1990**, *90*, 1407−1445.
(20) Flynn, G. W.; Parmenter, C. S.; Wodtke, A. M. Vibrational Energy Transfer. *J. Phys. Chem.* **1996**, *100*, 12817−12838.
(21) *Highly Excited Molecules: Relaxation, Reaction and Structure*; Mullin, A. S., Schatz, G. C., Eds.; ACS Symposium Series 678; American Chemical Society: Washington, DC, 1996.
(22) Hold, U.; Lenzer, T.; Luther, K.; Reihs, K.; Symonds, A. C. Collisional Energy Transfer Probabilities of Highly Excited Molecules from Kinetically Controlled Selective Ionization (KCSI). I. The KCSI Technique: Experimental Approach for the Determination of P(E′,E) in the Quasicontinous Energy Range. *J. Chem. Phys.* **2000**, *112*, 4076−4089.
(23) Grigoleit, U.; Lenzer, T.; Luther, K.; Mützel, M.; Takahara, A. Collisional Energy Transfer of Highly Vibrationally Excited Toluene and Pyrazine: Transition Probabilities and Relaxation Pathways from KCSI Experiments and Trajectory Calculations. *Phys. Chem. Chem. Phys.* **2001**, *3*, 2191−2202.
(24) Hold, U.; Lenzer, T.; Luther, K.; Symonds, A. C. Collisional Energy Transfer Probabilities of Highly Excited Molecules from KCSI. III. Azulene: P(*E*′,*E*) and Moments of Energy Transfer for Energies up to 40,000 cm-1 via Self-calibrating Experiments. *J. Chem. Phys.* **2003**, *119*, 11192−11211.
(25) Liu, C.-L.; Hsu, H. C.; Hsu, Y. C. Energy Transfer of Highly Vibrationally Excited Naphtalene. I. Translational Collision Energy Dependence. *J. Chem. Phys.* **2007**, *127*, 104311.
(26) Du, J.; Sassin, N. A.; Havey, D. K.; Hsu, K.; Mullin, A. S. Full State-Resolved Energy Gain Profiles of CO_2 from Collisions with Highly Vibrationally Excited Molecules. II. Energy-Dependent Pyrazine (E = 32700 and 37900 cm^{-1}) Relaxation. *J. Phys. Chem. A* **2013**, *117*, 12104−12115.

(27) Hold, U.; Lenzer, T.; Luther, K.; Reihs, K.; Symonds, A. Collisional Energy Transfer Probabilities in the Deactivation of Highly Vibrationally Excited Aromatics. *Ber. Bunsen.-Ges.* **1997**, *101*, 552−565.
(28) Wall, M. C.; Mullin, A. S. Supercollision" Energy Dependence: State-resolved Energy Transfer in Collisions Between Highly Vibrationally Excited Pyrazine (Evib = 37,900 cm-1 and 40,900 cm-1) and CO_2. *J. Chem. Phys.* **1998**, *108*, 9658−9667.
(29) Wall, M. C.; Lemoff, A. S.; Mullin, A. S. Independent Determination of Supercollision Energy Loss Magnitudes and Rates in Highly Vibrationally Excited Pyrazine with Evib = 36,000−41,000 cm-1. *J. Phys. Chem. A* **1998**, *102*, 9101−9105.
(30) Pashutzki, A.; Oref, I. Collision-induced Dissociation of Cyclohexadiene by a Vibrationally Hot Collider. *J. Phys. Chem.* **1988**, *92*, 178−182.
(31) Liu, C.-L.; Hsu, H. C.; Lyu, J.-J.; Ni, C.-K. Supercollisions and Energy Transfer of Highly Vibrationally Excited Molecules. *J. Chem. Phys.* **2005**, *123*, 131102.
(32) Jasper, A. W.; Miller, J. A. Collisional Energy Transfer in Unimolecular Reactions: Direct Classical Trajectories for $CH_4 \rightleftarrows CH_3$ + H in Helium. *J. Phys. Chem. A* **2009**, *113*, 5612−5619.
(33) Jasper, A. W.; Miller, J. A. Theoretical Unimolecular Kinetics for CH_4 +M ⇄ CH_3 + H + M in Eight Baths, M = He, Ne, Ar, Kr, H_2, N_2, CO, CH_4. *J. Phys. Chem. A* **2011**, *115*, 6438−6455.
(34) Jasper, A. W.; Miller, J. A.; Klippenstein, S. J. The Collision Efficiency of Water in the Unimolecular Reaction CH_4 (+H_2O) → CH_3 + H (+H_2O): One-Dimensional and Two-Dimensional Solutions of the Low-Pressure-Limit Master Equation. *J. Phys. Chem. A* **2013**, *117*, 12243−12255.
(35) Barker, J. R.; Weston, R. E., Jr. Collisional Energy Transfer Probability Densities P(E, J; E′, J′) for Monatomics Colliding with Large Molecules. *J. Phys. Chem. A* **2010**, *114*, 10619−10633. Barker, J. R.; Weston, R. E. Correction to "Collisional Energy Transfer Probability Densities P(E,J;E′,J′) for Monatomics Colliding with Large Molecules. *J. Phys. Chem. A* **2012**, *116*, 799−799.
(36) Brown, N. J.; Miller, J. A. Collisional Energy Transfer in the low-pressure limit: Unimolecular Dissociation of HO_2. *J. Chem. Phys.* **1984**, *80*, 5568−5580.
(37) Lendvay, G.; Schatz, G. C. Comparison of Master Equation and Trajectory Simulation of the Relaxation of an Ensemble of Highly Vibrationally Excited Molecules. *J. Phys. Chem.* **1994**, *98*, 6530−6536.
(38) Lenzer, T.; Luther, K.; Troe, J.; Gilbert, R. G.; Lim, K. F. Trajectory Simulations of Collisional Energy Transfer in Highly Excited Benzene and Hexafluorobenzene. *J. Chem. Phys.* **1995**, *103*, 626−641.
(39) Lim, K. F.; Gilbert, R. G. Calculation of Collisional-Energy-Transfer Rates in Highly Excited Molecules. *J. Phys. Chem.* **1990**, *94*, 72−77.
(40) Whyte, A. R.; Gilbert, R. G. A Classical Trajectory Calculation of Average Energy Transfer Parameters for the CH3OO + Ar System. *Aust. J. Chem.* **1989**, *442*, 1227−1234.
(41) Conte, R.; Houston, P. L.; Bowman, J. M. Communication: A Benchmark-quality, Full-dimensional ab initio Potential Energy Surface for Ar-HOCO. *J. Chem. Phys.* **2014**, *140*, 151101.
(42) Troe, J. Theory of Thermal Unimolecular reactions at low Pressures. I. Solutions of the Master Equation. *J. Chem. Phys.* **1977**, *66*, 4745−4757.
(43) Troe, J. Theory of Thermal Unimolecular reactions at low Pressures. II. Strong collision rate constants. Applications. *J. Chem. Phys.* **1977**, *66*, 4758−4775.
(44) Gilbert, R. G. Theory of collisional Energy Transfer of highly excited Molecules. *Int. Rev. Phys. Chem.* **1991**, *10*, 319−347.
(45) Barker, J. R.; Yoder, L. M.; King, K. D. Vibrational energy transfer modeling of nonequilibrium polyatomic reaction systems. *J. Phys. Chem. A* **2001**, *105*, 796−809.
(46) Marcus, R. A. Dissociation and Isomerization of Vibrationally Excited Species III. *J. Chem. Phys.* **1965**, *43*, 2658−2661.
(47) Gilbert, R. G.; Smith, S. C. *Theory of Unimolecular and Recombination Reactions*; Blackwell Scientific: Oxford, 1990.
(48) Smith, S. C.; Gilbert, R. G. Angular momentum Conservation in Unimolecular and Recombination Reactions. *Int. J. Chem. Kin.* **1988**, *20*, 307−329.
(49) Bernshtein, V.; Oref, I. Effect of Supercollisions on Chemical Reactions in the Gas Phase. *J. Phys. Chem.* **1993**, *97*, 12811−12818.
(50) Oref, I. Supercollisions. In *Vibrational Energy Transfer Involving Large and Small Molecules*; Barker, J. R., Ed.; JAI Press Inc.: Greenwich,CT, 1995; *Vol. 2B*; pp 285−298.
(51) Nordholm, S.; Freasier, B. C.; Jolly, D. L. Ergodic Collision Theory of Intermolecular Energy Transfer. *Chem. Phys. Lett.* **1977**, *25*, 433−449.
(52) Freasier, B. C.; Jolly, D. L.; Nordholm, S. ERgodic Collision Theory of Intermolecular Energy Transfer II. Quantum Effects in the Harmonic Approximation. *Chem. Phys.* **1978**, *32*, 161−168.
(53) Ming, L.; Sewell, T. D.; Nordholm, S. A Simulation Study of energy Transfer in Methyl Isocyanide-Inert Gas Collisions. *Chem. Phys.* **1995**, *199*, 83−104.
(54) Ming, L.; Davidsson, J.; Nordholm, S. Energy Transfer in Collisions of Small Gas-phase Clusters - Comparison of Molecular Dynamics and Statistical limit Estimates. *Chem. Phys.* **1995**, *201*, 121−140.
(55) Ming, L.; Davidsson, J.; Nordholm, S. Molecular Dynamics Study of Energy Transfer in Binary Collisions of Water Molecules. *J. Chem. Phys.* **1996**, *104*, 9001−9015.
(56) Nilsson, D.; Nordholm, S. Statistical model of energy transfer in molecular collisions: De-energization of highly excited toluene. *J. Chem. Phys.* **2002**, *116*, 7040−7048.
(57) Nilsson, D.; Nordholm, S. Modeling Energy Transfer in Molecular Collisions: Statistical Theory versus Experiment for Highly Excited Toluene and Azulene. *J. Chem. Phys.* **2003**, *119*, 11212−11220.
(58) Nilsson, D.; Nordholm, S. Statistical Theory of Collisional Energy Transfer in Molecular Collisions. Trans-Stilbene Deactivation by Argon, Carbon Dioxide, and n-Heptane. *J. Phys. Chem. A* **2006**, *110*, 3289−3296.
(59) Barker, J. R. A state-to-state statistical-dynamical theory for large molecule collisional energy transfer. Ber. Bunx. G. *Phys. Chem. Chem. Phys.* **1997**, *101*, 566−573.
(60) Lenzer, T.; Luther, K.; Nilsson, D.; Nordholm, S. PECT Model Analysis and Predictions of Experimental Collisional Energy Transfer Probabilities P(E′,E) and Moments (Delta E) for Azulene and Biphenylene. *J. Phys. Chem. B* **2005**, *109*, 8325−8331.
(61) Holbrook, K. A.; Pilling, M. J.; Robertson, S. H. *Unimolecular Reactions*, 2 ed.; Wiley: Chichester, 1996.
(62) Chemical Kinetics and Reaction Dynamics, Houston, P. L., (WCB/McGraw-Hill, New York, 2001). This book has now been reprinted by Dover, November 1, 2006, ISBN: 0486453340.
(63) Landau, L.; Teller, E. Zur Theorie der Schalldispersion. *Phys. Z. Sowjetunion* **1936**, *10*, 34.
(64) Nikitin, E. E.; Troe, J. 70 years of Landau-Teller theory for Collisional Energy Transfer. Semiclassical three-dimensional generalizations of the classical collinear model. *Phys. Chem. Chem. Phys.* **2008**, *10*, 1483−1501.
(65) Brunner, T. A.; Pritchard, D. E. Fitting Laws for Rotationally Inelastic Collisions. *Adv. Chem. Phys.* **1982**, *50*, 589.
(66) McCaffery, A. J.; Proctor, M. J.; Whitaker, B. J. Rotational Energy Transfer: Polarization and Scaling. *Annu. Rev. Phys. Chem.* **1986**, *37*, 223−244.
(67) Steinfeld, J. I.; Ruttenberg, P.; Millot, G.; Fanjoux, G.; Lavorel, B. Scaling laws for Inelastic Collision processes in Diatomic Molecules. *J. Phys. Chem.* **1991**, *15*, 9638−9647.
(68) Besley, N. A.; McCaffery, A. J.; A, O. M.; Zaid, R. Quantized momentum Mechanics of Inelastic and Reactive Collisions: the role of Energy and Angular Momentum Constraints. *J. Phys. B: At. Mol. Opt. Phys.* **1998**, *31*, 4267−4282.
(69) McCaffery, A. J.; Alwahabi, Z. T.; Osborne, M. A.; Williams, C. J. Rotational Transfer, an Angular Momentum Model. *J. Chem. Phys.* **1993**, *98*, 4586−4602.
(70) McCaffery, A. J. A new approach to molecular collision dynamics. *Phys. Chem. Chem. Phys.* **2004**, *6*, 1637−1657.

(71) Light, J. C. Phase Space Theory of Chemical Kinetics. *J. Chem. Phys.* **1964**, *40*, 3221−3229.
(72) Pechukas, P.; Light, J. C. On Detailed Balancing and Statistical Theories of Chemical Kinetics. *J. Chem. Phys.* **1965**, *42*, 3281−3291.
(73) Chen, C.; Braams, B.; Lee, D. Y.; Bowman, J. M.; Houston, P. L.; Stranges, D. Evidence for Vinylidene Production in the Photodissociation of the Allyl Radical. *J. Phys. Chem. Lett.* **2010**, *1*, 1875−1880.
(74) Chen, C.; Braams, B.; Lee, D. Y.; Bowman, J. M.; Houston, P. L.; Stranges, D. The Dynamics of Allyl radical Dissociation. *J. Phys. Chem. A* **2011**, *115*, 6797−6804.
(75) 8. Varandas, A. J. C.; Rodrigues, S. P. J. Double Many-Body Expansion Potential Energy Surface for Ground-State HCN Based on Realistic Long Range Forces and Accurate ab initio Calculations. *J. Chem. Phys.* **1997**, *106*, 9647−9658.
(76) Stranges, D.; O'Keeffe, P.; Scotti, G.; DiSanto, R.; Houston, P. L. Competing sigmatropic shift rearrangements in excited allyl radicals. *J. Chem. Phys.* **2008**, *128*, 151101.
(77) Boys, S. F.; Bernardi, F. The Calculation of small molecular Interactions by the differences of Separate Total Energies. Some Procedures with Reduced Errors. *Mol. Phys.* **1970**, *19*, 553−566.
(78) Lendvay, G.; Schatz, G. C. Observation of Highly Energetic Collisions in Classical Trajectory Studies of Collisional Energy Transfer. *J. Phys. Chem.* **1990**, *94*, 8864−8866.
(79) Pawlowski, F.; Jorgensen, P.; Olsen, J.; Hegelund, F.; Helgaker, T.; Gauss, J.; Bak, K. L.; Stanton, J. F. Molecular Equilibrium Structures from Experimental Rotational Constants and Calculated Vibration-Rotation Interaction Constants. *J. Chem. Phys.* **2002**, *116*, 6482−6496.
(80) Alexander, W. A.; Troya, D. Theoretical Study of the Ar-, Kr-, and Xe-CH_4, -CF_4 Intermolecular Potential Energy Surfaces. *J. Phys. Chem. A* **2006**, *110*, 10834−10843.
(81) Bosanac, S. Two-dimensional Model of Rotationally Inelastic Collisions. *Phys. Rev. A* **1980**, *22*, 2617−2622.
(82) Bosanac, S.; Buck, U. Rotational Rainbow Scattering from an Off-center Rigid Shell Model. *Chem. Phys. Lett.* **1981**, *81*, 315−319.